



HAL
open science

Legacy-micropollutant contamination levels in major river basins based on findings from the Rhône Sediment Observatory

Hugo Delile, André-marie Dendievel, Anice Yari, Matthieu Masson, Cecile Mieke, Brice Mourier, Marina Coquery

► To cite this version:

Hugo Delile, André-marie Dendievel, Anice Yari, Matthieu Masson, Cecile Mieke, et al.. Legacy-micropollutant contamination levels in major river basins based on findings from the Rhône Sediment Observatory. *Hydrological Processes*, 2022, 36 (2), pp.e14511. 10.1002/hyp.14511 . hal-03589353

HAL Id: hal-03589353

<https://hal.science/hal-03589353>

Submitted on 2 Jan 2023

HAL is a multi-disciplinary open access archive for the deposit and dissemination of scientific research documents, whether they are published or not. The documents may come from teaching and research institutions in France or abroad, or from public or private research centers.

L'archive ouverte pluridisciplinaire **HAL**, est destinée au dépôt et à la diffusion de documents scientifiques de niveau recherche, publiés ou non, émanant des établissements d'enseignement et de recherche français ou étrangers, des laboratoires publics ou privés.

1 Legacy-micropollutant contamination levels in major river basins based on 2 findings from the Rhône Sediment Observatory

3 Hugo Delile^{1,2*}, André-Marie Dendievel³, Anice Yari¹, Matthieu Masson¹, Cécile Miège¹,
4 Brice Mourier³, Marina Coquery¹

5 ¹INRAE, UR RiverLy, 5 Rue de la Doua CS 20244, F-69625, Villeurbanne, France

6 ²Univ. Lyon, CNRS, Archéorient, UMR 5133, Maison de l'Orient et de la Méditerranée,
7 France

8 ³Univ. Lyon, Université Claude Bernard Lyon 1, CNRS, ENTPE, UMR 5023 LEHNA, F-
9 69518 Vaulx-en-Velin Cedex, France

10 *Corresponding author: hugo.delile@cnrs.fr

11 **KEYWORDS:** Micropollutant yields, Long-term monitoring program, Large river basins,
12 Anthropogenic pressures, Persistent Organic Pollutants, Trace Metal Elements

13 Abstract

14 For more than half a century, chemical contamination has progressively spread to all the world's
15 large river basins. Large river outlets integrate multiple anthropogenic pressures in watersheds,
16 making them the largest source of sediment-bound contaminants to continental shelf areas.
17 However, comparing particulate micropollutant contaminations between the large river basins
18 is a challenging task, especially due to the scarcity of long-term river monitoring programs.
19 Here we address this issue, with a focus on legacy particulate micropollutants
20 (polychlorobiphenyls [PCBi], polycyclic aromatic hydrocarbons [PAHs], and trace metal
21 elements [TME]) yields. For this purpose, we employed a bottom-up multiscale approach to
22 chemical contamination in river basins that takes micropollutant yields measured in the Rhône
23 River sub-basins (France) as a benchmark of other large river basins. Data on the Rhône River
24 basin came from a unique 10-year-long monitoring program within the Rhône Sediment
25 Observatory (OSR), and were compared to data gathered on 18 major worldwide river outlets.

1
2
3 26 The Rhône River basin is far cleaner now than a few decades ago, likely due to environmental
4
5 27 regulations. At a wider spatial scale, our results depict an overall contamination gradient
6
7 28 splitting the most heavily contaminated river basins, located in developing and industrializing
8
9 29 low-to-middle-income countries, from the least contaminated rivers located in developed high-
10
11 30 income countries. We argue that chemical contamination levels of large river basins depend on
12
13 31 their stage of economic development.
14
15

16 17 32 **1. INTRODUCTION**

18
19
20 33 For more than five decades, freshwaters worldwide have experienced large-scale chemical
21
22 34 deterioration, especially by legacy pollutants, to the extent that water quality concerns have
23
24 35 become a major challenge for humanity in the twenty-first century (Meybeck and Helmer, 1989;
25
26 36 Schwarzenbach et al., 2010; UNEP-DHI and UNEP, 2016; Damania et al., 2019). As a result,
27
28 37 over the last ten years, this chemical contamination issue has become part of a broader concept
29
30 38 called “planetary boundaries”. These environmental limits define “a safe operating space for
31
32 39 humanity” through nine processes regulating the stability and resilience of the Earth system
33
34 40 (Rockström et al., 2009). Nonetheless, chemical contamination remains unquantified within the
35
36 41 framework of this concept (Steffen et al., 2015; Lade et al., 2020). The general lack of large-
37
38 42 scale and long-term monitoring programs limits efforts to assess the chemical risk at local and
39
40 43 regional scales (e.g. Schwarzenbach et al., 2006; Steffen et al., 2015; Malaj et al., 2014), and is
41
42 44 therefore a bottleneck to global-level assessment of chemical contamination in freshwaters. In
43
44 45 a recent attempt to assess global river contamination, water quality was dealt with solely via
45
46 46 two main categories of pollutants: nutrients (nitrogen and phosphorous) and pathogens
47
48 47 (untreated human waste; UNEP-DHI and UNEP, 2016; Best, 2019; Damania et al., 2019).
49
49 48 However, more than 140,000 different chemicals have been synthesized since the mid-twentieth
50
50 49 century (Landrigan et al., 2018), which further complicates efforts to produce a global-level
51
52 50 assessment of chemical contamination in rivers.
53
54
55
56
57
58
59
60

1
2
3 51 Rivers, floodplains, and watersheds in general have all helped to support the development
4
5 52 of human societies, especially by supplying natural resources required for agro-pastoral,
6
7 53 industrial, urban, domestic and mining activities (e.g. Macklin and Lewin, 2015; Vianello,
8
9 54 2015; UNEP-DHI and UNEP, 2016; Best, 2019). In return, these anthropogenic activities have
10
11 55 released land-based organic and inorganic micropollutants into nearby rivers, which then
12
13 56 carried pollutants downstream to coastal plains (Meybeck, 2003; Schwarzenbach et al., 2006).
14
15 57 As a result, rivers ensure source-to-sink transport of sediment-bound micropollutants (Meybeck
16
17 58 and Helmer, 1989; Gioia et al., 2011; Gómez-Gutiérrez et al., 2006; Wang et al., 2007; Liu et
18
19 59 al., 2009; Delile et al., 2020). For these reasons, large river basin outlets can be seen as
20
21 60 integrators of multiple anthropogenic pressures in watersheds, and thus as a proxy for assessing
22
23 61 the global distribution of chemical contamination of upstream freshwaters.
24
25
26
27

28 62 Here we chose to focus on micropollutants that (i) remain a global concern due to their
29
30 63 ubiquity at worldwide scale and (ii) are preferentially transported on particles. In this respect,
31
32 64 suspended particulate matter (SPM) provides an integrated signal of particle-bound
33
34 65 micropollutant concentrations (Schwientek et al., 2013; Masson et al., 2018; Rügner et al.,
35
36 66 2019). The studied sediment-bound legacy contaminants are persistent organic pollutants
37
38 67 (POPs: polychlorobiphenyls [PCBi] and polycyclic aromatic hydrocarbons [PAHs]) and trace
39
40 68 metal elements (TME: arsenic - As, cadmium - Cd, cobalt - Co, chromium - Cr, copper - Cu,
41
42 69 mercury - Hg, nickel - Ni, lead - Pb and zinc - Zn), all of which are considered as global, legacy
43
44 70 contaminants (Schwarzenbach et al., 2010).
45
46
47
48

49 71 These contaminants are also known to be particularly harmful because of their toxic,
50
51 72 persistent, bioaccumulative, and/or lipophilic properties (Schwarzenbach et al., 2010). Their
52
53 73 main impacts on aquatic environments are loss of biodiversity and impairment of ecosystem
54
55 74 services (Beketov et al., 2013; Malaj et al., 2014; Rasmussen et al., 2012; Schäfer et al., 2013).
56
57
58
59
60

75 Their risks to human and animal health are primarily related to their carcinogenicity and
76 neurotoxic, genotoxic, and immunotoxic effects (Lauby-Secretan et al., 2013).

77 The main goal of this study is to assess releases of particle-bound chemicals by some of
78 the large river basins spread across five of continents using specific fluxes of legacy organic
79 and inorganic micropollutants, which we call “micropollutant yields”. We compared
80 contamination levels among the world’s large river basins (Europe: Rhône, Garonne, Loire,
81 Seine, Volga, Danube, Elbe, and Rhine; Asia: Pearl [Zhujiang], Liao, Yangtze [Changjiang],
82 Yellow [Huang He], Mekong, and Ganges-Brahmaputra; North America: Mississippi,
83 Colorado, and St. Lawrence; South America: Amazon; Africa: Niger) based on a bottom-up
84 multiscale river basins approach. In this bottom-up approach, we use a comprehensive and
85 unparalleled monitoring from one river basin (i.e., a benchmark) to provide an assessment of the
86 use of micropollutant yields as an indicator of river basin contamination. We used the medium-
87 sized Rhône River basin as a benchmark because it has highly resolved (spatial and temporal)
88 data on particulate micropollutant concentrations, fluxes and yields collected over a 10-year-
89 long monitoring program as part of the Rhône Sediment Observatory (OSR) (Poulier et al.,
90 2019; Delile et al., 2020). We also investigated the relationship between magnitude of
91 micropollutant contaminations and economic stages of development (Meybeck and Helmer,
92 1989; Shafik, 1994; Panayotou, 2000).

93 **2. DESIGNING A BOTTOM-UP MULTISCALE APPROACH TO ASSESS THE** 94 **RIVER-BASIN CONTAMINATION**

95 To assess contamination levels in major river basins spread around the globe, we developed a
96 bottom-up multiscale approach using particulate micropollutant yields as a consistent proxy for
97 inter-basin comparison of micropollutants contamination. Particulate micropollutant yields
98 were estimated as the total inter-annual volume of particulate micropollutant fluxes (kg or t

1
2
3 99 yr⁻¹) discharged at the river outlets weighted by the size (km²) of the river watersheds (Meybeck
4
5 100 and Helmer, 1989; Mäkelä and Meybeck, 1996; Babut et al., 2016; Delile et al., 2020).

6
7 101 We started by analyzing the contamination of the sub-basins of the Rhône River to
8
9 102 assess the spatial representativeness of this proxy at a larger scale, i.e. the whole Rhône River
10
11 103 basin. We then extrapolated this information on micropollutants contamination of the Rhône
12
13 104 River basin to other large French river basins (Loire, Garonne, and Seine) and major continental
14
15 105 river basins (Europe, Asia, North and South America, and Africa) to assess country- to
16
17 106 continental-scale freshwater chemical contamination. Finally, we performed an inter-continent
18
19 107 comparison of chemical contamination levels in large river basins.

20
21
22
23 108 This bottom-up multiscale river basins approach also helped us to unravel the major
24
25 109 drivers of micropollutant yields, especially sensitivity to SPM fluxes and land-use. Land cover
26
27 110 data on the Rhône River basin and its main sub-basins were derived from the Corine Land
28
29 111 Cover (CLC) year 2018-version database (EEA, 2020) and classified into eight major categories
30
31 112 (forests, agricultural land, shrub and/or grassy vegetation, bare areas, urban areas, industrial
32
33 113 and commercial areas, water bodies, and others). These categories were merged from the 44
34
35 114 categories available in the CLC. One of the most important issues addressed in this study is the
36
37 115 role played by the successive economic stages of development in shaping the magnitude of
38
39 116 legacy micropollutant-based contamination of the large river basins. Here again, the long-term
40
41 117 monitoring of the Rhône River basin enabled us to assess pluri-decadal temporal trends in
42
43 118 micropollutant pollution. We then compared these trends against the historical pattern of
44
45 119 economic development in the Rhône River basin since the 1980s. Finally, feedbacks identified
46
47 120 for the Rhône River basin allowed us to explore the interrelationship between economic
48
49 121 development stage and pollution magnitude at the scale of large river basins.

50
51 122 The several temporal scales required by the bottom-up multiscale approach implied
52
53 123 referring to three specific chronological series:
54
55
56
57
58
59
60

- 1
2
3 124 - The intra-decadal trends refer to the 2008–2019 period based on the dataset gathered
4
5 125 monthly or every two weeks by the OSR monitoring program. Trends are therefore
6
7 126 computed at a high temporal resolution (bi-monthly to monthly) but over a relatively
8
9
10 127 short period (around one decade);
11
12 128 - The inter-decadal trends refer to the 1980s–2010s period and a comparison of one
13
14 129 decade to the next. Trends are therefore computed at a low temporal resolution (one
15
16 130 decade) but over a relatively long period (four decades);
17
18
19 131 - The inter-annual temporal resolution refers to the average of each individual year for
20
21 132 the 2008–2018 period for the Rhône River basin and the 2000–2020 period for the
22
23 133 large river basins. We use the inter-annual data to address spatial rather than temporal
24
25
26 134 trends.

135 3. STUDY AREA

136 3.1. Monitoring context of the Rhône River basin

137 The Rhône River is the largest single source of freshwater (~18% of the total inputs)
138 (UNEP/MAP, 2003; Antonelli et al., 2008; Ludwig et al., 2009) and particulate matter (Qi et
139 al., 2014; Antonelli et al., 2008; Syvitski and Kettner, 2007) to the Mediterranean Sea. Water
140 and sediment are released by a complex hydrological regime, which comprises a tri-modal
141 distribution over the year, including snow and glacier melting (Isère River and the Upper Rhône
142 River), an oceanic pluvial regime (Saône River), and a Mediterranean component (Durance
143 River) (Pardé, 1925; Bravard and Clemens, 2008). The geological contrast of the Rhône River
144 basin is summarized by both its old western Hercynian crustal segments (240 Ma and older) of
145 the Massif Central, and its young eastern Alpine mountains (30–120 Ma) (Blichert-Toft et al.,
146 2016). Readers seeking further details on the geological and hydrological features of the Rhône
147 River basin are invited to see extensive description recently published by Dendievel et al.
148 (2020b).

1
2
3 149 Since 2009, the Rhône Sediment Observatory (OSR) has become the most extended and
4
5 150 in-depth sedimentary monitoring network in France, featuring integrative or high-frequency
6
7 151 measurements throughout the ~100,000 km² Rhône River basin (Fig. 1 A) of 1) particulate
8
9 152 organic and inorganic micropollutant concentrations, 2) SPM, and 3) water discharge (Poulier
10
11 153 et al., 2019). The monitoring network includes several sampling stations distributed along the
12
13 154 Rhône River and at the outlets of its main tributaries, from Lake Geneva to the Mediterranean
14
15 155 Sea (Fig. 1A). Two main stations are located directly on the French part of the Rhône River at
16
17 156 Jons and Arles/Beaucaire, and further secondary stations have been set up on its main tributaries
18
19 157 just upstream of their confluence with the Rhône River (Arve, Fier, Saône, Gier, Isère, Drôme,
20
21 158 Durance, Ardèche and Gardon Rivers) (Le Bescond et al., 2018; Thollet et al., 2021). We have
22
23 159 used data from the 10-year-long OSR to accurately quantify the inter-annual (2008–2018)
24
25 160 average particulate micropollutant fluxes discharged into the Mediterranean Sea, decipher their
26
27 161 seasonal dynamics within the Rhône River catchment, and estimate the specific contributions
28
29 162 of the main tributaries (Delile et al., 2020). In this study, we focused on stations in the Upper
30
31 163 Rhône River (Jons), the Saône River, the Gier River, the Isère River, the Durance River, and
32
33 164 the Rhône River outlet (Arles/Beaucaire) (Fig. 1A and Tab. S1), as they have the longest
34
35 165 monitoring history (Poulier et al., 2019). The six stations cover 80% of the watershed area
36
37 166 (~96,500 km²) (Fig. 1 and Tab. S1).

167 3.2. Defining the major worldwide river basins investigated

168 There has been extensive discussion in the scientific literature on which indicator best describes
169 river size (river length, drainage basin area, water discharge, etc.; Best, 2019). The “world’s
170 large rivers” considered in this paper are those that have a river basin area greater than 100,000
171 km² (Meybeck and Helmer, 1989), and that host large populations (Tab. 1). There are more than
172 250 rivers worldwide with drainage basins larger than 100,000 km². However, by considering
173 the sum of the population hosted in each of the 19 river basins considered in this study (□ 2

1
2
3 174 billion inhab.) and their respective annual sediment flux discharges ($\approx 4,000 \text{ Mt yr}^{-1}$), the 19
4
5 175 basins taken together account for around $\approx 30\%$ of the global population (≈ 7 billion inhab.)
6
7
8 176 and fluvial sediment discharge ($13,000 \text{ Mt yr}^{-1}$) (Syvitski et al., 2005; Syvitski and Kettner,
9
10 177 2011; Bravard, 2018) (Tab. 1). This selection of large rivers was also based on the availability
11
12 178 of data on the sediment fluxes and concentrations of the targeted particulate micropollutants
13
14 179 (PCB, PAH, and TME) at the river outlets, and on the selected economic indicators (population,
15
16
17 180 urbanization, Gross Domestic Product [GDP], dams) (data sources shown in Tab. 1).

181 4. METHODS

182 In this section, we define the study area, the datasets used to compute the temporal trends of
183 the Rhône River basin and the inter-annual particulate micropollutant yields of the large river
184 basins.

185 4.1. Assessment of temporal trends in particulate micropollutant concentrations and 186 fluxes at the Rhône River outlet

187 We describe here the methodology used to assess temporal trends (1980s-2010s) in particulate
188 micropollutant concentrations (C_{micropol}) and fluxes (F_{micropol}), and SPM fluxes (F_{SPM}) at the
189 Rhône River outlet. Sub-section 4.1.1. describes the data and statistical tests used to assess the
190 temporal evolution in chemical water quality at the Rhône River outlet at inter-decadal (1980s–
191 2010s period) and intra-decadal (2008–2019 period) resolution (Tab. 2). Then, in sub-section
192 4.1.2., we describe the methodology used to calculate the inter-decadal micropollutant
193 concentrations and fluxes (1980s–2010s). In section 2.4, we describe the inter-annual
194 micropollutant yields calculated over the 2008–2018 period.

195 4.1.1. River sediment matrices used and statistical tests

196 The inter- and intra-decadal resolution of temporal trends in particulate micropollutant
197 concentrations and fluxes at the Rhône River outlet since the 1980s is based on two datasets
198 (Tab. 2 and Fig. S1):

1
2
3 199 - prior to 2008–2010, TME, PAHs and PCB_i data came from research labs and monitoring
4
5 200 agencies studying deposited sediments, i.e. bed and flood deposits, and sediment cores;
6
7
8 201 - after 2008–2010, TME, PAHs and PCB_i data came primarily from SPM measured under
9
10 202 the OSR monitoring program. A small amount of data acquired on deposited sediments
11
12 203 was also used to build a composite record for the 2010–2019 period.

14 204 The dataset used to assess inter-decadal trends includes several types of sediment matrices
15
16
17 205 (Tab. 2) that are likely to affect micropollutant concentrations (effect of grain-size distribution
18
19 206 and/or organic matter concentrations). For this reason, in figure S1, we compared
20
21 207 micropollutant concentrations between suspended (SPM) and deposited sediments (including
22
23 208 bed and flood deposits, and sediment cores) for the 2010–2019 period. Overall, organic
24
25 209 micropollutant concentrations were \square 25% lower in SPM than in deposited sediments, whereas
26
27 210 TME were 30% to 100% higher in SPM. Even though these differences are not negligible,
28
29 211 concentrations remain similar in magnitude and were used for the assessment of the inter-
30
31 212 decadal trends. However, the dataset used for the assessment of intra-decadal trends was
32
33 213 exclusively from SPM sediments (Tab. 2), since at this fine temporal scale, mixing various
34
35 214 sediment matrices would undermine the results.

37
38
39 215 Micropollutant concentrations data were gathered from the lower part of the Rhône River
40
41 216 (Arles/Beaucaire station, i.e. 120 kilometers from the Rhône River outlet) for TME (Cd, Cr,
42
43 217 Cu, Hg, Ni, Pb and Zn), 7 indicator PCB_i (congeners 28, 52, 101, 118, 138, 153, and 180; noted
44
45 218 Σ_7 PCB, and 12 priority PAHs (anthracene, benz[a]anthracene, benzo[a]pyrene,
46
47 219 benzo[b]fluoranthene, benzo[ghi]perylene, benzo[k]fluoranthene, chrysene,
48
49 220 dibenz[a,h]anthracene, fluoranthene, indeno[1,2,3-cd]pyrene, phenanthrene, pyrene; denoted
50
51 221 with the abbreviation Σ_{12} PAH). All of these data were produced by monitoring authorities (the
52
53 222 Rhône–Mediterranean–Corsica water agency) and the OSR monitoring program. Our database
54
55
56
57
58
59
60

1
2
3 223 includes several particulate matrices, i.e. bed and flood deposits, SPM and sediment cores.
4
5 224 Additional sediment core data came from various research labs (Tab. 2).
6

7
8 225 More specifically, PAH data from bed and flood sediments over the period 1994–1997
9
10 226 were available from the Rhône–Mediterranean–Corsica water agency (data source:
11
12 227 <http://www.naiades.eaufrance.fr>) (Tab. 2), whereas PAH data for SPM come from the OSR
13
14 228 dataset over the period 2011–2016 (Delile et al., 2020; Thollet et al., 2021). The TME and
15
16 229 Σ_7 PCB analyses are available since the 1980s (Tab. 2) based on data for sediment cores and bed
17
18 230 and flood deposits (see Dendievel et al., 2020a,b for details on the data, stations and methods
19
20 231 used). Over the periods 2011–2018 for TME and 2008–2017 for PCB_i, we only used SPM data
21
22 232 from the OSR dataset (Delile et al., 2020; Thollet et al., 2021). Arsenic (As) and cobalt (Co)
23
24 233 were only measured since the 2010s in the OSR program and were not measured in previous
25
26 234 decades (Tab. 2).
27
28
29

30 235 To decipher temporal trends in micropollutant concentrations and mean monthly water
31
32 236 discharges data during the past decade, we used HYPE software for trends identification of
33
34 237 time-series (Croiset and Lopez, 2013). We used the non-parametric Mann-Kendall test for
35
36 238 identifying monotonic trends over the entire duration of time-series because micropollutant
37
38 239 concentrations data were not normally-distributed. We used the modified Mann-Kendall test
39
40 240 (Hamed and Rao, 1998) because (i) each micropollutant data time-serie has more than 40
41
42 241 analyses and (ii) the test is valid for assessment of autocorrelation in time-series data. Only the
43
44 242 statistically significant temporal trends (p-value < 0.05) over to the total length of the time-
45
46 243 series are presented. Furthermore, two-steps structural break tests were performed for each
47
48 244 micropollutant time-series. Firstly, we applied the non-parametric Pettitt's test (Pettitt, 1979)
49
50 245 derived from the Mann-Whitney test to detect a change of average in time-series. The tipping
51
52 246 point was considered statistically significant when the p-value of the test was less than 5%.
53
54 247 Secondly, we used the non-parametric Darken's test (Darken, 1999; Darken et al., 2000) to
55
56
57
58
59
60

1
2
3 248 identify a trend reversal in time-series consisting in a change of the sign of a slope. Trend
4
5 249 reversal Darken test compares the Kendall's tau for two sections in time-series. If the p-value
6
7
8 250 is less than 5%, then the micropollutant series includes a significant trend reversal, and the
9
10 251 break dates are determined.

11 12 252 **4.1.2. Calculation of temporal trends in particulate micropollutant concentrations and** 13 14 253 **fluxes**

15
16
17 254 The calculation of inter-decadal particulate micropollutant fluxes at the Rhône River outlet is
18
19 255 summarized below in three steps.

20
21 256 Firstly, TME concentrations in sediment cores were measured using an *Aqua Regia*
22
23 257 digestion (hydrochloric acid - 3N HCl and nitric acid - HNO₃) (Dendievel et al., 2020c), and
24
25 258 bed, flood and SPM sediment samples were analyzed using a total extraction (HCl, HNO₃, H₂O₂
26
27 259 and hydrofluoric acid - HF) (see Delile et al., 2020 for the detailed analytical procedure).
28
29
30 260 Thus, in order to combine and compare these data, TME concentrations from sediment cores
31
32 261 were corrected according to the relationships between these two types of extractions as
33
34 262 proposed by Dendievel et al. (2020c). From these legacy micropollutants datasets, we computed
35
36 263 inter-decadal trends (1980s-2010s) for the particulate micropollutant concentrations.

37
38
39 264 Second, we reconstructed the inter-decadal SPM fluxes since the 1980s. We used the SPM
40
41 265 data systematically measured under the OSR program since 2011, but a reconstruction was
42
43 266 needed for the earlier periods without regular measurement. Thus, based on the known water
44
45 267 discharge for each month (available at <http://www.hydro.eaufrance.fr>), the SPM concentrations
46
47 268 (mg L⁻¹) and fluxes (Mt yr⁻¹) were reconstructed using the specific rating curves and equations
48
49 269 published by Poulier et al. (2019) for the Rhône River.

50
51
52 270 Third, we calculated the inter-decadal micropollutant fluxes (1980s–2010s). These fluxes
53
54 271 were computed by multiplying the SPM fluxes (step 2) by the decadal median of the
55
56 272 micropollutant concentrations resulting from both monitoring series (from the Rhône–
57
58
59
60

1
2
3 273 Mediterranean–Corsica water agency on bed and flood sediments, and from the OSR
4
5 274 monitoring program on SPM), and dated sediment cores (Tab. 2).

7 275 **4.2. Assessment of the Rhône River basin’s inter-annual micropollutant yields**

9
10 276 The inter-annual micropollutant yields computed as specific micropollutant fluxes (g or kg km^{-2}
11
12 yr^{-1} , i.e. the micropollutant fluxes weighted by the watershed size), provide an integrative
13
14 277 estimation of the chemical contamination level of the river basin. First, to assess the inter-annual
15
16 278 average micropollutant fluxes over the 2008–2018 period, we calculated the SPM fluxes as the
17
18 279 product of hourly measured data on both water discharges and SPM concentrations at each
19
20 280 station in the OSR (Fig. 1 and Tab. S1). Second, micropollutant fluxes were calculated by
21
22 281 multiplying the SPM fluxes by monthly time-integrated and flow-proportional particulate
23
24 282 micropollutant concentrations obtained from particle traps (Schulze et al., 2007; Masson et al.,
25
26 283 2018; Poulhier et al., 2019; Delile et al., 2020) or by a continuous flow centrifuge (for the
27
28 284 Arles/Beaucaire station only). Masson et al. (2018) compared micropollutant concentrations
29
30 285 measured by both SPM sampling methods at the Jons station (draining the Upper Rhône River
31
32 286 basin, Fig. 1) and did not find statistically significant between-method differences, which
33
34 287 suggests that these SPM sampling systems are comparable. Data for micropollutants with a
35
36 288 quantification frequency (QF) $< 50\%$ were not considered in the present study (4 priority
37
38 289 PAHs). For some other organic micropollutants (PCBi and PAHs), data that were below the
39
40 290 limit of quantification (LOQ) were changed to LOQ/2 for calculation of micropollutant fluxes.
41
42 291 Readers seeking further details on the micropollutant fluxes computation, and especially about
43
44 292 the filling of non-monitored periods or gaps in the measurement time-series of both SPM and
45
46 293 micropollutant concentrations and the estimation of flux uncertainties, are invited to see the
47
48 294 extensive description by Delile et al. (2020). Third, the inter-annual particulate micropollutant
49
50 295 fluxes at the mouth of the Rhône River (Arles/Beaucaire station) and its main tributaries (Saône
51
52 296 River, Upper Rhône River, Gier River, Isère River and Durance River; Fig. 1 and Tab. S1) were
53
54
55
56
57
58
59
60

1
2
3 298 weighted by the corresponding watershed size to get the micropollutant yields (g or kg km⁻² yr⁻¹
4
5 299 for POPs or TME, respectively) at the Rhône River basin and sub-basin scales.
6
7

8
9 300 **4.3. Assessment of the inter-annual micropollutants yields of the world's large river**
10
11 301 **basins**

12
13 302 To assess micropollutant yields, we estimated the annual sediment fluxes discharged at
14
15 303 the outlet of the selected rivers. Accurate estimation of sediment fluxes remains a challenging
16
17 304 issue (Mouyen et al., 2018; Poulier et al., 2019; Hackney et al. 2020), especially at global scale,
18
19 305 because less than 10% of the river mouths worldwide have monitoring of sediment delivery
20
21 306 (Syvitski et al., 2005; Bravard, 2018). In addition, *in-situ* sediment discharge measurements are
22
23 307 highly uncertain (spatially sparse and temporally discontinuous data, different-measurement
24
25 308 time frequencies, heterogeneous measuring techniques) (Mouyen et al., 2018). We therefore
26
27 309 used the modeled annual fluvial sediment fluxes (Nienhuis et al., 2020) for all of the large rivers
28
29 310 included in this study (Tab. 1). These data were produced using WBMSed (Cohen et al., 2013,
30
31 311 2014) and BQART (Kettner and Syvitski, 2008) methods. This approach using modelled
32
33 312 estimates of sediment flux at the large river outlets appears particularly suitable for our study,
34
35 313 since it catches the multiyear average sediment fluxes as well as inter-annual and intra-annual
36
37 314 trends (Cohen et al., 2013).
38
39
40
41
42

43 315 Then, annual micropollutant fluxes were calculated by multiplying the sediment fluxes
44
45 316 by the median concentration of each micropollutant (Fig. S2) for each river on the basis of
46
47 317 sediment samples collected at the outlet of the rivers. Based on our homemade micropollutant
48
49 318 concentrations database, Table S2 shows specific concentrations (median and range) of
50
51 319 micropollutants (mg or µg kg⁻¹ dry weight), inter-annual particulate micropollutant fluxes (kg
52
53 320 or t yr⁻¹), yields (g or kg km⁻² yr⁻¹) and per capita data (mg or g inhab⁻¹ yr⁻¹) for 19 large rivers
54
55 321 spread among five continents. The references used to establish this database are detailed in
56
57 322 Supplementary Text. All the data gathered on our homemade micropollutant concentrations
58
59
60

1
2
3 323 database come from sediment samples collected over the 2000–2020 period and refer to several
4
5 324 sediment matrices including surface, bed and flood deposits, SPM, and sediment cores. Data
6
7
8 325 sources (Supplementary Text) include data and scientific papers (e.g., Dendievel et al., 2020a,b,
9
10 326 c), academic studies (e.g. Masson, 2007), databases of river monitoring surveys (e.g. OSR for
11
12 327 the Rhône River, <https://bdoh.irstea.fr/OBSERVATOIRE-DES-SEDIMENTS-DU-RHONE/>;
13
14 328 the IKSr-CIPR-ICBR program for the Rhine River, <http://iksr.bafg.de/iksr/auswahl.asp?S=1>;
15
16 329 the HYBAM observatory for the Amazon River, <http://www.ore-hybam.org>), and institutional
17
18 330 organizations (e.g. French water agencies, data source: <http://www.naiades.eaufrance.fr>). Our
19
20 331 database contains sediment samples collected at the outlet of the rivers in order to get an
21
22 332 integrative signal of the watershed. In addition, particular attention was paid to exclude
23
24 333 sampling stations potentially affected by mixing with saline oceanic or estuarine waters.
25
26 334 Regarding PAHs and PCBi, for each sample, we either directly compiled available data on the
27
28 335 sum of the 16 priority PAHs (INERIS, 2005) and the sum of the 7 indicator PCBi congeners,
29
30 336 or manually calculated these sums using available data on individual chemicals. The 16 priority
31
32 337 PAHs are not systematically available in the scientific literature or other data sources: indeed,
33
34 338 the number of priority PAHs initially measured ranges from 12 to 16 PAH. Consequently,
35
36 339 results are shown as Σ_{12-16} PAH. For this reason, but also given the great diversity of the data
37
38 340 collected and the resulting uncertainties in sediment flux estimates, the computed
39
40 341 micropollutant yields of large river basins were classified according to 3 or 4 orders of
41
42 342 magnitude. Thus, the spatial distribution of the Σ_{12-16} PAH yields, for instance, was divided in
43
44 343 three order-of-magnitude classes, i.e. (1) 1–10, (2) 10–100 and (3) >100 g km⁻² yr⁻¹.
45
46
47
48
49
50
51

52 344 **5. RESULTS**

53
54
55 345 We present in this section results on the temporal and spatial trends of contamination in the
56
57 346 Rhône River basin and on the assessment of the relationship between the micropollutants
58
59 347 yields and SPM yields of large river basins.
60

348 5.1. Temporal trends in the Rhône River basin contamination

349 5.1.1. Long-term trends in micropollutant contamination since the 1980s

350 Figure 2 shows the pluri-decadal trends in particulate micropollutant concentrations and
 351 fluxes and SPM fluxes during the last 40 years at the Rhône River outlet. Table 3 presents
 352 specific variations (in percent) of micropollutant concentrations and fluxes and SPM fluxes
 353 from one decade to the next, noted $\Delta C_{\text{micropol}}$, $\Delta F_{\text{micropol}}$ and ΔF_{SPM} , respectively. The general
 354 time-course of micropollutant concentrations and fluxes follows a similar decreasing trend
 355 between 1980s–1990s: -58% for $\Delta C_{\Sigma 7\text{PCB}}$ and -69% for $\Delta F_{\Sigma 7\text{PCB}}$, and -42% for mean ΔC_{TME} and
 356 -57% for mean ΔF_{TME} .

357 After the 1990s, the organic and inorganic micropollutant concentrations and fluxes
 358 follow distinct patterns. POPs continued to decline in similar and stable proportions, both in
 359 concentrations (1990s to 2010s, $\Delta C_{\Sigma 7\text{PCB}} \square -39\%$, and $\Delta C_{\Sigma 12\text{PAH}} \square -38\%$ on average) and fluxes
 360 (1990s to 2010s, $\Delta F_{\Sigma 7\text{PCB}} \square -37\%$, and $\Delta F_{\Sigma 12\text{PAH}} \square -35\%$ on average) (Fig. 2A-D and Tab. 3).
 361 The time-course of PCB and PAH fluxes over the period reproduces the same pattern as the
 362 concentrations. In contrast to the POPs, TME fluxes showed a similar pattern of change to the
 363 SPM flux trend. TME and SPM fluxes decreased significantly with similar rank order of
 364 magnitude between the 1990s–2000s ($\Delta F_{\text{TME}} \square -34\%$ and $\Delta F_{\text{SPM}} \square -28\%$), whereas ΔC_{TME}
 365 decreased slightly ($\square -8\%$) over the same period. Thereafter, TME and SPM fluxes increased
 366 sharply between 2000 and 2010s ($\Delta F_{\text{TME}} \square +21\%$ and $\Delta F_{\text{SPM}} \square +44\%$) while ΔC_{TME}
 367 experienced a slight decline ($\square -8\%$) (Fig. 2E-F and Tab. 3).

368 The relative weights of C_{micropol} and F_{SPM} in F_{micropol} variations from one decade to the
 369 next were assessed (see Tab. 3) by comparing (i) the decadal variations (in %) of inter-annual
 370 particulate micropollutant concentrations (ΔC) and fluxes (ΔF), and SPM flux and (ii) their
 371 respective correlation coefficients. We defined three micropollutant groups by assessing the

weight of $\Delta C_{\text{micropol}}$ and ΔF_{SPM} in $\Delta F_{\text{micropol}}$: (1) concentration-driven micropollutant fluxes for $\Sigma_7\text{PCB}$, $\Sigma_{12}\text{PAH}$, Cd, Cr and Hg (orange cells, and statistically significant correlation coefficients of F_{micropol} vs. C_{micropol} in Tab. 3), (2) SPM flux-driven micropollutant fluxes for Cu and Ni (grey cells, and statistically significant correlation coefficients of F_{micropol} vs. F_{SPM} in Tab. 3), and (3) alternately concentration-driven and SPM flux-driven micropollutant fluxes for Pb and Zn (orange and grey cells, and statistically significant correlation coefficients of F_{micropol} vs. C_{micropol} and of F_{micropol} vs. F_{SPM} in Tab. 3). According to Table 3, SPM flux-driven micropollutant fluxes switch to concentration-driven micropollutant fluxes when $\Delta C_{\text{micropol}}$ is higher than $\pm 30\%$. In other words, variations of micropollutant concentrations have to vary by more than 30% in order to affect micropollutant fluxes. Below this threshold, SPM fluxes primarily control micropollutants fluxes.

5.1.2. Short-term trends in micropollutant contamination over the past decade

Figure 3 shows the temporal evolution of particulate micropollutant concentrations at the Arles station (Rhône River outlet, Fig. 1) over the past decade (2010s). Mean monthly water discharges and associated temporal trends over the total length of the time-series are also shown in order to capture the relationship between the water discharge trends and the micropollutant concentrations trends. Overall, the results highlight three micropollutant trend groups: (1) increasing concentrations for As, Co, Cr, Ni and Zn, (2) decreasing concentrations for $\Sigma_7\text{PCB}$, and (3) no trend for $\Sigma_{12}\text{PAH}$, Cd, Cu, Hg and Pb (Fig. 3). Given that the mean monthly water discharge does not show statistically significant temporal trends, it cannot lead to an increase or decrease in micropollutant concentration trends.

The comparison between the increase in annual rates of TME concentrations (red values in Fig. 3) of the first group (As, Co, Cr, Ni and Zn) and their respective median value (Tab. S2) indicates an average annual rate of increase of 7% per year.

1
2
3 396 The second trend group (2) concerns Σ_7 PCB concentrations, which over the total length
4
5 397 of the time-series (2008-2016) decreased at a mean annual rate of $1.4 \mu\text{g kg}^{-1}$ (i.e. -9% per year;
6
7 398 Fig. 3). This trend is in line with the general pattern of decreasing PCB contamination of the
8
9 399 Rhône River waters that began in the 1990s (Desmet et al., 2012; Mourier et al., 2014; Babut
10
11 400 et al., 2016; Liber et al., 2019; Dendievel et al., 2020a) (Fig. 2A). Nonetheless, the trend showed
12
13 401 a change-point in October 2013, with a slight increase in PCB concentrations of about $+1.6 \mu\text{g}$
14
15 402 kg^{-1} per year (i.e. +9%) (Fig. 3).
16
17
18
19

20 403 **5.2. Spatial trend in Rhône River basin contamination**

21
22
23 404 Figure 4 is a map of the particulate micropollutants yields of the whole Rhône River basin
24
25 405 and its main sub-basins. It shows a sharp contrast between a less contaminated area in the North
26
27 406 (Saône River and Upper Rhône River basins) and a more contaminated area in the South (Isère
28
29 407 River, Gier River and Durance River basins). This contrast appears more clearly for TME
30
31 408 yields, which have a spatial distribution pattern that matches the features of intra-basin SPM
32
33 409 yields (Fig. 4). As a result, TME yields in the different tributaries seem to be sensitive to
34
35 410 variation in SPM yields. The SPM yields in the Rhône River basin come mainly from the Isère
36
37 411 and Durance river basins, since they are known to be the largest suppliers of the inter-annual
38
39 412 SPM flux discharged into the Mediterranean Sea from the Rhône River outlet. Each of these
40
41 413 two tributaries accounts for 31% of the total inter-annual SPM flux of the Rhône River, while
42
43 414 the Upper Rhône River, Saône River and Gier River account for 11%, 6%, and 0.1%,
44
45 415 respectively (Delile et al., 2020).
46
47
48
49
50

51 416 Figure 5 is a Principal Component Analysis (see details on the PCA method in the
52
53 417 Supplementary Text) combining the micropollutants yields, population density and land use of
54
55 418 each station (Fig. 1B). The first principal component (F1 ~ 56%) results from the contribution
56
57 419 of all micropollutants yields, meaning that F1 tracks the overall contamination level. However,
58
59
60

1
2
3 420 the contribution of mean TME yields to the F1 component (7.5%) is twice as large as the
4
5 421 contribution of organic micropollutants (2.7%). Organic micropollutants are more involved in
6
7 422 the F2 positive values, since PAH and PCB yields contribute on average about 8% to the F2
8
9 423 component (only 2.5% for mean TME contribution). The F2 axis shows a striking contrast
10
11 424 between anthropogenic land use (positive values) as agricultural lands, urban areas and
12
13 425 industrial and commercial areas (ICA) on one side and natural land use (forests, bare, and
14
15 426 shrub/vegetation) (negative values) on the other (Fig. 5). Population density is highly correlated
16
17 427 to urban areas and ICA ($R > 0.93$ and 0.89 , respectively; p -value < 0.05). Based on the F2
18
19 428 component, TME yields divide into two groups: first, a natural land use-related TME group
20
21 429 with Cr, Co, Ni and Hg, and a second anthropogenic land use-related TME group with As, Pb,
22
23 430 Zn, Cd and Cu (Fig. 5). In addition, the first TME group is significantly correlated with SPM
24
25 431 fluxes (R values 0.93 – 0.98 ; p -value < 0.05), which is not the case for the second group (R
26
27 432 values 0.48 – 0.68 ; p -value > 0.05). The location of the river stations into the PCA differentiates
28
29 433 the northern and southern areas of the Rhône River basin: the Upper Rhône and Saône rivers in
30
31 434 the north showing the lowest micropollutant yields, and the Isère and Durance rivers in the
32
33 435 south characterized by natural land use and SPM flux-bound TME yields. The Gier River
34
35 436 appears to be the most contaminated basin, especially for organic micropollutants yields (Fig.
36
37 437 4), and also the most impacted by anthropogenic land use (Figs.1 and 5).

438 **5.3. Assessment of the relationship between the micropollutant yields and SPM yields** 439 **of the large river basins**

440 Building upon our findings from the Rhône River basin on the main patterns of micropollutant
441 yields, we next extrapolated that knowledge of SPM fluxes to assess micropollutant yield signal
442 of the large river basins. The maps of micropollutant yields show that some TME yields follow
443 spatial trends of SPM yields (Fig. S3), whereas PAH and PCB yields seem unconstrained by
444 SPM yields (Fig. 6). River basins in high-income countries (i.e. Europe and North America)

1
2
3 445 show the lowest SPM yields ($< 66 \text{ t km}^2 \text{ yr}^{-1}$) (except for the Rhine River basin), while river
4
5 446 basins in low-income countries (i.e. Asia and South America) show the highest SPM yields ($>$
6
7 447 $100 \text{ t km}^2 \text{ yr}^{-1}$) (except for the Niger River basin) (Figs. 6 and S3, and Tab. 1).

8
9
10 448 The potential control of SPM fluxes on micropollutant yields was assessed through the
11
12 449 correlation circle of the PCA (Fig. 7A, see details on the PCA method in the Supplementary
13
14 450 Text) and the correlation matrices between micropollutant and SPM yields (Tab. S3), and
15
16 451 between micropollutant yields and median concentrations (Tab. S4). We identified three groups
17
18 452 of micropollutant yields:

- 19
20
21 453 1) Anthropogenic activity-driven PCB, PAH, Cd and Hg yields: uncorrelated with SPM
22
23 454 yields ($R \square 0.15-0.40$, $p\text{-value} > 0.05$), and positively correlated to their median
24
25 455 concentrations ($R \square 0.6-0.8$, $p\text{-value} < 0.05$);
26
27
28 456 2) SPM flux-driven Co, Cr, Ni and Cu yields: positively correlated to SPM yields ($R \square$
29
30 457 $0.8-1$, $p\text{-value} < 0.05$), and uncorrelated with their median concentrations ($R \square 0.2-0.3$,
31
32 458 $p\text{-value} > 0.05$);
33
34
35 459 3) Anthropogenic activity/SPM flux-driven As, Zn and Pb yields: positively correlated to
36
37 460 SPM yields ($R \square 0.5-0.8$, $p\text{-value} < 0.05$) and to their median concentrations ($R \square 0.5-$
38
39 461 0.6 , $p\text{-value} < 0.05$).

42 462 **6. DISCUSSION**

44 463 **6.1. Insights from the bottom-up multiscale approach to assess the river-basin** 45 46 464 **contamination**

47
48
49
50 465 The assessment of the Rhône River's intra-basin contamination has shown a striking spatial
51
52 466 heterogeneity between the northern and southern areas of the Rhône River basin. For instance,
53
54 467 except for Zn, the first group of TME concentrations (As, Co, Cr, Ni and Zn) of the Rhône
55
56 468 River basin matches the specific chemical fingerprint of the Isère River's SPM (Delile et al.,
57
58 469 2020). We can therefore assume a process of enhanced soil erosion in specific Isère River sub-
59
60

1
2
3 470 basins on Ni, Co and Cr element-rich geological basements, leading to increasing
4
5 471 concentrations of these TME over the past decade (2010s). However, only additional TME
6
7 472 geochemical tracing methods, such as Pb, Cu and Zn isotopic fingerprinting techniques (Bird,
8
9 473 2011) or geochemical fingerprinting (Bégorre et al., 2021; Dabrin et al., 2021), could capture
10
11 474 specific sources of TME in sediments. This heterogeneous pattern of the micropollutant yields
12
13 475 of the Rhône River basin suggests that calculated micropollutants yields of the large river basins
14
15 476 need to be considered with caution, in terms of the sources of the chemical fluxes. Such fluxes
16
17 477 should not be considered as uniformly deposited over the entire surface of the river basins. Our
18
19 478 reconstructions of the temporal trends of particulate micropollutant concentrations and fluxes
20
21 479 at the Rhône River outlet since the 1980s show that micropollutant concentrations have to vary
22
23 480 by more than 30% to affect micropollutant fluxes. As a result, this threshold defines the switch
24
25 481 from SPM flux-driven to anthropogenic pressure-driven micropollutant yields. Applied to the
26
27 482 other 18 large river basins worldwide, this balance between micropollutant concentrations and
28
29 483 SPM fluxes suggests a progressive anthropogenic origin of the micropollutant yields as follows:
30
31 484 (i) SPM flux-driven Co, Cr, Ni and Cu yields, (ii) anthropogenic activity and SPM flux-driven
32
33 485 As, Zn and Pb yields, and (iii) anthropogenic activity-driven PCB, PAH, Cd and Hg yields.
34
35
36
37
38
39

40 486 It is striking to note that these large river basins-bound micropollutant yield groups are
41
42 487 close to those identified in the Rhône River sub-basins since PCB, PAH, As, Pb, Zn, Cd and
43
44 488 Cu yields are related to their contamination level, while Cr, Co, Ni and Hg yields are more
45
46 489 related to their SPM yields. Only Hg and Cu yields do not belong to the same group. This is a
47
48 490 key point. We argue that the diversity of the geological basements of the Rhône River sub-
49
50 491 basins captured in Rhône Sediment Observatory data is the decisive factor for explaining this
51
52 492 distinction between Hg and Cu yields.
53
54
55
56

57 493 As a result, regarding TME, the lack of geochemical background data for each river basin
58
59 494 is a significant barrier to considering TME yields as a consistent proxy for assessing river basin
60

1
2
3 495 contamination. Indeed, as it stands, TME yields reflect a mixture comprising both the TME
4
5 496 fraction coming from the local geological environment and TME fraction from the
6
7 497 anthropogenic activity. Therefore, TME yields would be more suitable to track anthropogenic
8
9 498 contamination of river basins if local geological effects on TME yields could be removed.
10
11 499 Nevertheless, the clustering of TME demonstrates that the proportion of natural and
12
13 500 anthropogenic inputs is not the same for all TME. Indeed, at the worldwide river basins scale,
14
15 501 the anthropogenic source is the dominant contributor to Hg and Cd whereas the natural source
16
17 502 is the dominant contributor to Ni, Co, Cr and Cu. The Rhône River monitoring network data
18
19 503 shows the tipping-point switch from a predominantly natural to anthropogenic TME yields
20
21 504 requires TME concentrations that are \approx 30% higher than the local geochemical backgrounds.
22
23
24
25
26

27 505 **6.2. Role of economic development on the global distribution of micropollutants yields**

28
29 506 Considering all micropollutant yields, the distribution of the large river basins within the PCA
30
31 507 defines three statistically-based mixing lines showing a gradient of overall contamination level
32
33 508 from the least contaminated river basins in the bottom-left corner of the graph up to the most
34
35 509 contaminated river basins in the upper-right part of the graph (Fig. 7B). The slope mixing lines
36
37 510 depend of the relative weight between the anthropogenic origin of the micropollutant yields
38
39 511 (Group 1-based mixing line) and the contribution of SPM fluxes to micropollutant yields
40
41 512 (Groups 1 + 2 +3-based mixing line). The mixing lines split river basins into two groups: the
42
43 513 most contaminated rivers located in developing countries (Asia and South America), and the
44
45 514 least contaminated rivers located in developed countries (Europe and North America).
46
47
48
49

50
51 515 Based on the long-term trends of the Rhône River basin contamination, it appears that the
52
53 516 overall chemical contamination level during the 1980s was similar to that currently observed in
54
55 517 countries undergoing economic transition. According to previous works, the highest
56
57 518 contamination levels, tied to the developing low-to-middle-income countries, result from
58
59
60

1
2
3 519 increasing demand for both energy required for petroleum-powered vehicles and electricity
4
5 520 generation and natural resources (e.g., mining) or else from deforestation due to intensive
6
7 521 agriculture (Schwarzenbach et al., 2010; Landrigan et al., 2018). This growing demand for
8
9 522 energy and natural resources is driven by uncontrolled growth of cities and large-scale
10
11 523 urbanization in these countries (Wilkinson et al., 2007; UNESCO, 2009; Shen et al., 2013).

12
13
14
15 524 The environmental quality improvement of the Rhône River basin during the 2010s is
16
17 525 apparent as a leftward shift in Figure 8 towards the cluster of less-contaminated rivers. This
18
19 526 substantial decline since the 1980s is part of a global decline in POPs (Breivik et al., 2002a,b
20
21 527 and 2007 for PCB; Shen et al., 2011, 2013 for PAH) and TME releases (McConnell et al., 2019;
22
23 528 Legrand et al., 2020). This decline may result from national (see French regulation timeline for
24
25 529 PCB_i in Fig. 2) and international implementations of environmental regulations (e.g. PCB_i
26
27 530 listed in the Stockholm Convention [UNEP, 2001] and PAHs in the Aarhus Protocol on
28
29 531 Persistent Organic Pollutants [United Nations, 1998]) in many developed countries (Miller and
30
31 532 Orbock Miller, 2007). Indeed, other studies have shown that the lower contamination level of
32
33 533 the river basins located in developed countries results from (i) efforts to mitigate industrial,
34
35 534 municipal and household wastewaters, (ii) the commissioning of sanitation and water supply
36
37 535 infrastructures, and (iii) national and international environmental regulations on emissions
38
39 536 control and the use of chemical products (UNESCO, 2009; Schwarzenbach et al., 2010; UNEP-
40
41 537 DHI and UNEP, 2016; Landrigan et al., 2018; Damania et al., 2019).

42
43
44
45
46
47
48 538 This general model seems to show an environmental quality improvement depending on
49
50 539 successive economic stages of development. Such a trend fits rather well with the theoretical
51
52 540 framework of the Environmental Kuznets Curve (EKC) (Grossman and Krueger, 1991, 1995;
53
54 541 Shafik and Bandyopadhyay, 1992). According to EKC theory, this relationship, which is
55
56 542 assumed to take the form of an inverted U-shape curve, comes from a period of environmentally
57
58 543 damaging economic growth followed by improvement in environmental quality as per capita

1
2
3 544 income and/or GDP rises. However, this theory has been criticized due to, for example, the
4
5 545 unsuitable statistical analyses of time-series (Stern et al., 1996; Stern, 2004) or the
6
7 546 environmental and economic activity indicators on which it is based (Dinda, 2004).
8
9

10 547 **6.3. Comparison of the contamination levels in the world's large river basins**

11
12
13 548 The observed relationship between country income level and SPM yield derives from
14
15 549 well-known anthropogenic stresses such as agriculture-induced deforestation and river
16
17 550 damming (Syvitski and Kettner, 2011; Bravard, 2018; Nienhuis et al., 2020).
18
19

20 551 Polycyclic aromatic hydrocarbons and TME yields mapping well depict the relevance of
21
22 552 consumption of natural resources and energy for the economic development of our modern
23
24 553 societies (Figs. 6 and S3). In both cases, the highest micropollutant yields of Asian countries
25
26 554 (Figs. 6 and 8) are consistent with their atmospheric micropollutant emissions, since they
27
28 555 contribute around 50% of the global $\sum_{16}\text{PAH}$ (Shen et al., 2013) and TME emissions (Pacyna
29
30 556 and Pacyna, 2001). It has been estimated that almost two thirds of the global $\sum_{16}\text{PAH}$ emissions
31
32 557 come from residential/commercial burning of biomass, and this source accounts for about 80%
33
34 558 of emissions from South-East Asia (Shen et al., 2013). As underlined above, recent surging
35
36 559 urbanization is considered as the main driver of this high PAH contamination in developing
37
38 560 countries, because it results from extensive use of biomass for cooking and heating but also
39
40 561 from petroleum consumption by road vehicles (Shen et al., 2011, 2013). River basins in Western
41
42 562 Europe and North America show lower PAH yields (Figs. 6 and 8) thanks to the implementation
43
44 563 of emissions reduction technologies (Shen et al., 2011, 2013) and a series of legislative policies
45
46 564 in force since the 1970s, first with the 1979 Convention on Long-Range Transboundary Air
47
48 565 Pollution (CLRTAP) (UNECE, 1979) and then the Aarhus Protocol on POPs (United Nations,
49
50 566 1998). The implementation of this regulatory framework has brought about a sharp decrease in
51
52 567 $\sum_{12}\text{PAH}$ yields in the Rhône River basin, from 100.5 g km⁻² yr⁻¹ in the 1990s to 34.6 g km⁻² yr⁻¹
53
54 568 in the 2010s. However, the Rhine and Elbe river basins show similar PAH yield levels to those
55
56
57
58
59
60

1
2
3 569 of Asian countries. The heavy industrial legacy of the Rhine and Elbe river basins (Heise et al.,
4
5 570 2004; Förstner et al., 2004) could explain the high PAH contamination of these areas.
6
7

8 571 The spatial distribution pattern of TME yields is broadly similar to that of PAH, with the
9
10 572 highest levels found in Asia, followed by river basins in Europe and North America. However,
11
12 573 the Amazon River basin shows an equal if not higher level of TME contamination than river
13
14 574 basins in Europe and North America (Figs. 6 and 8). Once again, this pattern is consistent with
15
16 575 worldwide TME emissions estimates, since Asia accounts for between 40% and 60% of the
17
18 576 total depending on the TME, followed by Europe, North America and South America which
19
20 577 contribute between 10% and 20% depending on the TME (Pacyna and Pacyna, 2001; Streets et
21
22 578 al., 2017; Kubier et al., 2019). The two main sources of Hg, Cd, As, Zn, Cu, and Ni
23
24 579 contamination are non-ferrous metal production and non-vehicle fossil fuel combustion
25
26 580 (Pacyna and Pacyna, 2001; Streets et al., 2017). For example, during the 1990s, gold mining in
27
28 581 the Brazilian Amazon released around 130 t of Hg into the environment every year, of which
29
30 582 about half of that amount reached surface waters (Pfeiffer et al., 1993; Lacerda and Salomons,
31
32 583 1998). By adding the other minor anthropogenic Hg sources (e.g. chemicals manufacturing,
33
34 584 electrical and measuring equipment, Cu, Zn and Pb smelting, silver (Ag) production, coal and
35
36 585 oil combustion, etc.), the calculated Hg emission yield of $11 \text{ g km}^{-2} \text{ yr}^{-1}$ is close to our appraisal
37
38 586 of $12 \text{ g km}^{-2} \text{ yr}^{-1}$ (Table S2) and to other estimates, such as $9.3 \text{ g km}^{-2} \text{ yr}^{-1}$ (Fostier et al., 2000)
39
40 587 or $7\text{-}17 \text{ g km}^{-2} \text{ yr}^{-1}$ (Roulet et al., 1999) for the Amazon River basin. This comparison shows
41
42 588 that annual Hg yields derived from atmospheric emission and river outlet-bound particulate
43
44 589 fluxes are able to accurately track the magnitude of river basin contamination.
45
46
47
48
49

50
51 590 Finally, the spatial distribution of the PCBs yields over the large river basins is more
52
53 591 homogeneous than the other micropollutant yields, mainly because river basins in Asian
54
55 592 countries do not have the highest contamination levels (PCBi yields $\square 0.1$ to $10 \text{ g km}^{-2} \text{ yr}^{-1}$),
56
57 593 which are of the same order of magnitude as that of river basins of the developed countries
58
59
60

1
2
3 594 (PCBi yields $\square < 0.1$ to $10 \text{ g km}^{-2} \text{ yr}^{-1}$; Figs. 6 and 8). This pattern is in line with the global
4
5 595 pattern of PCB production and usage, which occurred mainly in North America and Europe
6
7 596 (Breivik et al., 2002a; Desforges et al., 2018), while Asian countries, especially China, had only
8
9 597 used PCB for a relatively short period (1965-1974) before they were banned. Only the South-
10
11 598 Eastern coast of China has been significantly impacted (Xu et al., 2000; Mai et al., 2005; Xing
12
13 599 et al., 2011).

14
15
16
17 600 Our assessment is limited by particulate micropollutant fluxes that originate from the
18
19 601 remobilization of contaminated sediments stored in rivers. For instance, the slight increase in
20
21 602 PCB concentrations since 2013 at the Rhône River outlet could result from a potential
22
23 603 remobilization of highly PCB-contaminated legacy sediments trapped within the alluvial
24
25 604 margins leading to the persistence of PCBi in the Rhône River waters (Babut et al., 2016; Liber
26
27 605 et al., 2019; Poulhier et al., 2019; Delile et al., 2020). Legacy contaminants reintroduced into the
28
29 606 river by physical processes (dam failure, greater flooding due to climate change, river
30
31 607 restoration programs, etc.) (Noyes et al., 2009; Eschbach et al., 2018; Cornwall, 2020) and/or
32
33 608 chemical processes (increasing solubility of some micropollutants; Stigliani, 1991;
34
35 609 Schwartzman et al. 2010) are likely to confound the relationship between economic
36
37 610 development phases and freshwater quality due to lag times (decadal to millennial time scales).
38
39 611 Legacy contaminated sediments along the river continuum pertain to the issue of (i)
40
41 612 contaminant residence times along river corridors (Pizzuto, 2014; Sutfin and Wohl, 2019;
42
43 613 Wohl, 2015, 2019), (ii) total time for contaminant transfer to river outlets, and (iii) the
44
45 614 theoretical decontamination time of a river basin (Singer et al., 2013; Gateuille et al., 2014,
46
47 615 2020).

54 55 616 7. CONCLUSIONS

56
57 617 We compared contamination levels in the large river basins using particulate micropollutant
58
59 618 yields, which were explored through a bottom-up multiscale river basins approach. In this

1
2
3 619 respect, we compared micropollutant yields based on a unique dataset from a 10-year-long-
4
5 620 monitoring program on the Rhône River sub-basins, then extrapolated up this approach to other
6
7 621 major river basins in order to assess the spatial representativeness of this chemical
8
9 622 contamination proxy.

10
11
12
13 623 Our reconstructions of the temporal trends of particulate micropollutant concentrations
14
15 624 and fluxes at the Rhône River outlet since the 1980s show that micropollutant concentrations
16
17 625 have to vary by more than 30% over 10 years to affect micropollutant fluxes. As a result, this
18
19 626 threshold defines the tipping point marking the switch from SPM flux-driven to anthropogenic
20
21 627 pressure-driven micropollutant yields. Applied to the other 18 large river basins worldwide, this
22
23 628 balance between micropollutant concentrations and SPM fluxes suggests a progressive
24
25 629 anthropogenic origin of the micropollutant yields as follows: (i) SPM flux-driven Co, Cr, Ni
26
27 630 and Cu yields, (ii) anthropogenic activity and SPM flux-driven As, Zn and Pb yields, and (iii)
28
29 631 anthropogenic activity-driven PCB, PAH, Cd and Hg yields. The distribution of the magnitude
30
31 632 of chemical contamination in the large river basins is related to the economic development stage
32
33 633 of the local country. Our results show an overall contamination gradient splitting the most
34
35 634 contaminated river basins in developing and industrializing low-income and middle-income
36
37 635 countries (Asia and South America) from the least contaminated rivers in developed high-
38
39 636 income countries (Europe and North America). This kind of spatial pattern in surface waters-
40
41 637 related chemical contamination fits well with the Environmental Kuznets Curve theory. Indeed,
42
43 638 our results show how a prevailing model of economic development implies rampant
44
45 639 urbanization supported by both increasingly high energy and natural resource consumption. In
46
47 640 turn, these conditions constitute major sources of chemical contamination in the world's large
48
49 641 river basins. In this respect, the long-term trend of contamination in the Rhône River basin
50
51 642 shows an overall chemical contamination level in the 1980s that was similar to levels observed
52
53 643 today in countries undergoing economic transition (Asia and South America). Then, starting in
54
55
56
57
58
59
60

1
2
3 644 the 1980s, chemical contamination levels of the Rhône River basin decreased, like the river
4
5 645 basins in other developed countries, leading to improvement in water quality.
6
7

8 646 Large river monitoring is needed worldwide, with a special focus on river outlets and
9
10 647 sustained monitoring for accurate global-level assessment of chemical contamination. In
11
12 648 addition to the legacy micropollutants investigated in the present study, we also need to consider
13
14 649 emerging chemicals (e.g. persistent mobile toxic substances), some of which need to be
15
16 650 monitored in the dissolved fraction. Finally, we feel that there is a need for consistent data on
17
18 651 geochemical background levels of TME for all of the world's large river basins, which would
19
20 652 help to get a sharper picture of anthropogenic TME-related river basin contamination. All of
21
22 653 these future developments could be implemented into watershed management plans to produce
23
24 654 a standard of proof required to conclude that the EKC theory is indeed a correct explanation of
25
26 655 the observed trends and could therefore be used to predict watershed trends worldwide.
27
28
29

30 656 **ACKNOWLEDGMENTS**

31
32
33 657 This study was conducted within the Rhône Sediment Observatory (OSR), a multi-partner
34
35 658 research program funded through the Plan Rhône by the European Regional Development Fund
36
37 659 (ERDF), Agence de l'eau RMC, CNR, EDF, and three French regional councils (Auvergne-
38
39 660 Rhône-Alpes, PACA, and Occitanie). We are grateful to the INRAE colleagues Alexandra
40
41 661 Gruat, Ghislaine Grisot, Mickaël Lagouy, Jérôme Le Coz, Aymeric Dabrin and Laurent Valette
42
43 662 for their assistance with SPM sampling, field campaigns, sample treatment, chemical analysis,
44
45 663 data analysis, and GIS analysis. We also thank Julie Gattacceca from the CEREGE laboratory,
46
47 664 and Hugo Lepage and Olivier Radakovitch from the IRSN laboratory for coordinating the SPM
48
49 665 sampling for the southern Rhône River stations and the ETM analyses (except Hg). Finally, we
50
51 666 wish to thank the four anonymous reviewers and Stephen Sebestyen, guest editor, for greatly
52
53 667 improving the manuscript.
54
55
56
57
58
59

60 668 **REFERENCES**

- 1
2
3 669 AERMC. 2019. Tableau de bord du SDAGE Rhône-Méditerranée 2016-2021 : bilan à mi-
4
5 670 parcours (in French). Available at: https://www.eaurmc.fr/jcms/pro_95600/fr/tableau-
6
7 671 [de-bord-du-sdage-rhone-mediterranee-2016-2021-bilan-a-mi-parcours](https://www.eaurmc.fr/jcms/pro_95600/fr/tableau-de-bord-du-sdage-rhone-mediterranee-2016-2021-bilan-a-mi-parcours) [Accessed on
8
9 672 [18 August 2020](#)]
- 10
11
12 673 Antonelli C, Eyrolle F, Rolland B, Provansal M, Sabatier F. 2008. Suspended sediment and
13
14 674 ¹³⁷Cs fluxes during the exceptional December 2003 flood in the Rhone River, southeast
15
16 675 France. *Geomorphology* **95** (3): 350–360
- 17
18
19 676 Babut M, Persat H, Desmet M, Lopes, Mourier B, Tronczynski J. 2016. Les PCB dans le Rhône.
20
21 677 In: *PCB, Environnement et Santé*, Paris; 473–498.
- 22
23
24 678 Bégorre C, Dabrin A, Morereau A, Lepage H, Mourier B, Masson M, Eyrolle F, Coquery M.
25
26 679 2021. Relevance of using the non-reactive geochemical signature in sediment core to
27
28 680 estimate historical tributary contributions. *Journal of Environmental Management*
29
30 681 **292**: 112775
- 31
32
33 682 Beketov MA, Kefford BJ, Schäfer RB, Liess M. 2013. Pesticides reduce regional biodiversity
34
35 683 of stream invertebrates. *Proceedings of the National Academy of Sciences* **110** (27):
36
37 684 11039–11043
- 38
39
40 685 Best J. 2019. Anthropogenic stresses on the world's big rivers. *Nature Geoscience* **12** (1): 7–
41
42 686 21
- 43
44
45 687 Bird G. 2011. Provenancing anthropogenic Pb within the fluvial environment: Developments
46
47 688 and challenges in the use of Pb isotopes. *Environment International* **37** (4): 802–819
- 48
49 689 Blichert-Toft J, Delile H, Lee C-T, Stos-Gale Z, Billström K, Andersen T, Hannu H, Albarède
50
51 690 F. 2016. Large-scale tectonic cycles in Europe revealed by distinct Pb isotope provinces.
52
53 691 *Geochemistry, Geophysics, Geosystems* **17** (10): 3854–3864
- 54
55
56 692 Bravard J.-P 2018. *Crises sédimentaires du globe. 1, Grands cours d'eau, de l'abondance à la*
57
58 693 *rareté*. ISTE éditions: London (in French).
59
60

- 1
2
3 694 Bravard, J-P, Clemens, A. 2008. *Le Rhône en 100 questions*. Zone Atelier Bassin du Rhône
4
5 695 (ZABR), Villeurbanne, France (in French) ; 295 p
6
7
8 696 Breivik K, Sweetman A, Pacyna JM, Jones KC. 2002a. Towards a global historical emission
9
10 697 inventory for selected PCB congeners — a mass balance approach: 1. Global production
11
12 698 and consumption. *Science of The Total Environment* **290** (1): 181–198
13
14
15 699 Breivik K, Sweetman A, Pacyna JM, Jones KC. 2002b. Towards a global historical emission
16
17 700 inventory for selected PCB congeners — a mass balance approach: 2. Emissions.
18
19 701 *Science of The Total Environment* **290** (1): 199–224
20
21
22 702 Breivik K, Sweetman A, Pacyna JM, Jones KC. 2007. Towards a global historical emission
23
24 703 inventory for selected PCB congeners — A mass balance approach: 3. An update.
25
26 704 *Science of The Total Environment* **377** (2): 296–307
27
28
29 705 Cohen S, Kettner AJ, Syvitski JPM. 2014. Global suspended sediment and water discharge
30
31 706 dynamics between 1960 and 2010: Continental trends and intra-basin sensitivity.
32
33 707 *Global and Planetary Change* **115**: 44–58
34
35
36 708 Cohen S, Kettner AJ, Syvitski JPM, Fekete BM. 2013. WBMsed, a distributed global-scale
37
38 709 riverine sediment flux model: Model description and validation. *Computers &*
39
40 710 *geosciences* **53**: 80–93
41
42
43 711 Cornwall W. 2020. A dam big problem. *Science* **369** (6506): 906–909
44
45
46 712 Croiset N, Lopez B. 2013. HYPE : Outil d’analyse statistique des séries temporelles d’évolution
47
48 713 de la qualité des eaux souterraines HYPE : Outil d’analyse statistique des séries
49
50 714 temporelles d’évolution de la qualité des eaux souterraines. Manuel d’utilisation RP-
51
52 715 63066-FR. BRGM (in French). <http://infoterre.brgm.fr/rapports/RP-63066-FR.pdf>
53
54
55 716 Dabrin A, Bégorre C, Bretier M, Dugué V, Masson M, Le Bescond C, Le Coz J, Coquery M.
56
57 717 2021. Reactivity of particulate element concentrations: apportionment assessment of
58
59 718 suspended particulate matter sources in the Upper Rhône River, France. *Journal of*
60

- 1
2
3 719 *Soils and Sediments* **21**: 1256-1274
4
5 720 Damania R, Desbureaux S, Rodella A-S, Russ J, Zaveri E. 2019. *Quality Unknown : The*
6
7 721 *Invisible Water Crisis*. Washington, DC: World Bank.
8
9 722 Darken P.F. (1999). Testing for changes in trend in water quality data. PhD Faculty of Virginia
10
11 723 Polytechnic Institute and State University.
12
13 724 Darken PF, Holtzman GI, Smith EP, Zipper CE. 2000. Detecting changes in trends in water
14
15 725 quality using modified Kendall's tau. *Environmetrics* **11**: 423-434
16
17 726 Delile H, Masson M, Miège C, Le Coz J, Poulhier G, Le Bescond C, Radakovitch O, Coquery
18
19 727 M. 2020. Hydro-climatic drivers of land-based organic and inorganic particulate
20
21 728 micropollutant fluxes: The regime of the largest river water inflow of the Mediterranean
22
23 729 Sea. *Water Research* **185**: 116067
24
25 730 Dendievel A-M, Mourier B, Coynel A, Evrard O, Labadie P, Ayrault S, Debret M, Koltalo F,
26
27 731 Copard Y, Faivre Q, et al. 2020a. Spatio-temporal assessment of the PCB sediment
28
29 732 contamination in the four main French River Basins (1945-2018). *Earth System Science*
30
31 733 Data Discussions: 1–23
32
33 734 Dendievel A-M, Mourier B, Dabrin A, Delile H, Coynel A, Gosset A, Liber Y, Berger J-F,
34
35 735 Bedell J-P. 2020b. Metal pollution trajectories and mixture risk assessed by combining
36
37 736 dated cores and subsurface sediments along a major European river (Rhône River,
38
39 737 France). *Environment International* **144**: 106032
40
41 738 Dendievel A-M, Mourier B, Dabrin A, Barra A, Bégorre C, Delile H, Hammada M, Lardaux
42
43 739 G, Berger J-F. 2020c. Dataset of natural metal background levels inferred from pre-
44
45 740 industrial palaeochannel sediment cores along the Rhône River (France). *Data in Brief*
46
47 741 **32**: 106256
48
49 742 Desforges J-P, Hall A, McConnell B, Rosing-Asvid A, Barber JL, Brownlow A, De Guise S,
50
51 743 Eulaers I, Jepson PD, Letcher RJ, et al. 2018. Predicting global killer whale population
52
53
54
55
56
57
58
59
60

- 1
2
3 744 collapse from PCB pollution. *Science* **361** (6409): 1373–1376
4
5 745 Desmet M, Mourier B, Mahler BJ, Van Metre PC, Roux G, Persat H, Lefèvre I, Peretti A,
6
7 746 Chapron E, Simonneau A, et al. 2012. Spatial and temporal trends in PCBs in sediment
8
9 747 along the lower Rhône River, France. *Science of The Total Environment* **433**: 189–197
10
11
12 748 Dinda S. 2004. Environmental Kuznets Curve Hypothesis: A Survey. *Ecological Economics* **49**
13
14 749 (4): 431–455
15
16
17 750 European Environment Agency (EEA), 2020. Corine Land Cover (CLC) 2018, v. 2020_20u1.
18
19 751 URL: <https://land.copernicus.eu/pan-european/corine-land-cover/clc2018>
20
21 752 Eschbach D, Schmitt L, Imfeld G, May J-H, Payraudeau S, Preusser F, Trauerstein M,
22
23 753 Skupinski G. 2018. Long-term temporal trajectories to enhance restoration efficiency
24
25 754 and sustainability on large rivers: an interdisciplinary study. *Hydrology and Earth*
26
27 755 *System Sciences* **22** (5): 2717–2737
28
29
30 756 Fostier AH, Forti MC, Guimarães JR, Melfi AJ, Boulet R, Espirito Santo CM, Krug FJ. 2000.
31
32 757 Mercury fluxes in a natural forested Amazonian catchment (Serra do Navio, Amapá
33
34 758 State, Brazil). *The Science of the Total Environment* **260** (1–3): 201–211
35
36
37 759 Förstner U, Heise S, Schwartz R, Westrich B, Ahlf W. 2004. Historical Contaminated
38
39 760 Sediments and Soils at the River Basin Scale. *Journal of Soils and Sediments* **4** (4):
40
41 761 247
42
43
44 762 Gateuille D, Evrard O, Lefevre I, Moreau-Guigon E, Alliot F, Chevreuil M, Mouchel J-M.
45
46 763 2014. Mass balance and decontamination times of Polycyclic Aromatic Hydrocarbons
47
48 764 in rural nested catchments of an early industrialized region (Seine River basin,
49
50 765 France). *Science of The Total Environment* **470–471**: 608–617
51
52
53 766 Gateuille D, Gasperi J, Briand C, Moreau-Guigon E, Alliot F, Blanchard M, Teil M-J,
54
55 767 Chevreuil M, Rocher V, Azimi S, et al. 2020. Mass Balance of PAHs at the Scale of
56
57 768 the Seine River Basin. In: Flipo N., Labadie P., Lestel L. (eds) *The Seine River Basin*.
58
59
60

- 1
2
3 769 The Handbook of Environmental Chemistry, vol 90: 163–188
4
5 770 Gioia R, Dachs J, Nizzetto L, Berrojalbiz N, Galba C, Del Vento S, Méjanelle L, Jones KC.
6
7 771 2011. Sources, Transport and Fate of Organic Pollutants in the Oceanic Environment.
8
9 772 In *Persistent Pollution – Past, Present and Future*. M. Quante, R. Ebinghaus, G. Flöser.
10
11 773 Springer Berlin Heidelberg, 111–139.
12
13 774 Gómez-Gutiérrez AI, Jover E, Bodineau L, Albaigés J, Bayona JM. 2006. Organic contaminant
14
15 775 loads into the Western Mediterranean Sea: estimate of Ebro River inputs. *Chemosphere*
16
17 776 **65** (2): 224–236
18
19 777 Grossman, GM, & Krueger, AB 1991. Environmental impacts of a North American Free Trade
20
21 778 Agreement. National Bureau of Economic Research Working Paper 3914, NBER,
22
23 779 Cambridge MA. <https://www.nber.org/papers/w3914>
24
25 780 Grossman, GM, & Krueger, AB 1995. Economic Growth and the Environment. The *Quarterly*
26
27 781 *Journal of Economics* **110** (2): 353–377
28
29 782 Hackney CR, Darby SE, Parsons DR, Leyland J, Best JL, Aalto R, Nicholas AP, Houseago RC.
30
31 783 2020. River bank instability from unsustainable sand mining in the lower Mekong
32
33 784 River. *Nature Sustainability* **3** (3): 217–225
34
35 785 Hamed KH & Rao AR, 1998. A modified Mann-Kendall trend test for autocorrelated data.
36
37 786 *Journal of Hydrology* **204** (1-4): 182-196
38
39 787 Heise S, Förstner U, Westrich B, Jancke T, Karnahl J, Salomons W, Schönberger H. 2004.
40
41 788 Inventory of historical contaminated sediment in Rhine Basin and its tributaries. Report
42
43 789 on Behalf of the Port of Rotterdam, p. 223
44
45 790 Immerzeel WW, Bierkens MFP. 2012. Asia's water balance. *Nature Geoscience* **5**: 841–842
46
47 791 INERIS. 2005. Hydrocarbures Aromatiques Polycycliques. Guide méthodologique.
48
49 792 Acquisition des données d'entrée des modèles analytiques ou numériques de transferts
50
51 793 dans les sols et les eaux souterraines. DRC – 66244 – DESP – R01 (in French).
52
53
54
55
56
57
58
59
60

- 1
2
3 794 INSEE. The National Institute of Statistics and Economic Studies Available at:
4
5 795 <https://www.insee.fr/fr/accueil> [Accessed on 8 October 2020] (in French)
6
7
8 796 Kammerer JC. 1990. Largest rivers in the United States. Report 87–242. USGS, Department of
9
10 797 the interior.
11
12 798 Kettner AJ, Syvitski JPM. 2008. HydroTrend v.3.0: A climate-driven hydrological transport
13
14 799 model that simulates discharge and sediment load leaving a river system. *Computers &*
15
16 800 *Geosciences* **34** (10): 1170–1183
17
18
19 801 Kubier A, Wilkin RT, Pichler T. 2019. Cadmium in soils and groundwater: A review. *Applied*
20
21 802 *Geochemistry* **108**: 104388
22
23
24 803 Lacerda LD de, Salomons W. 1998. Mercury from gold and silver mining: a chemical time
25
26 804 bomb? Springer: Berlin, New York.
27
28 805 Lade SJ, Steffen W, de Vries W, Carpenter SR, Donges JF, Gerten D, Hoff H, Newbold T,
29
30 806 Richardson K, Rockström J. 2020. Human impacts on planetary boundaries amplified
31
32 807 by Earth system interactions. *Nature Sustainability* **3** (2): 119–128
33
34
35 808 Landrigan PJ, Fuller R, Acosta NJR, Adeyi O, Arnold R, Basu N (Nil), Baldé AB, Bertollini
36
37 809 R, Bose-O'Reilly S, Boufford JI, et al. 2018. The Lancet Commission on pollution and
38
39 810 health. *The Lancet* **391** (10119): 462–512
40
41
42 811 Lauby-Secretan B, Loomis D, Grosse Y, El Ghissassi F, Bouvard V, Benbrahim-Tallaa L,
43
44 812 Guha N, Baan R, Mattock H, Straif K, et al. 2013. Carcinogenicity of polychlorinated
45
46 813 biphenyls and polybrominated biphenyls. *The Lancet. Oncology* **14** (4): 287–288
47
48
49 814 Le Bescond C, Thollet F, Poulier G, Gairoard S, Lepage H, Branger F, Jamet L, Raidelet N,
50
51 815 Radakovitch O, Dabrin A, et al. 2018. Des flux d'eau aux flux de matières en suspension
52
53 816 et de contaminants associés : gestion d'un réseau de stations hydro-sédimentaires sur le
54
55 817 Rhône. *La Houille Blanche* (3): 63–70 (in French).
56
57
58 818 Legrand M, McConnell JR, Lestel L, Preunkert S, Arienzo M, Chellman NJ, Stohl A, Eckhardt
59
60

- 1
2
3 819 S. 2020. Cadmium pollution from zinc-smelters up to fourfold higher than expected in
4
5 820 Western Europe in the 1980s as Revealed by Alpine Ice. *Geophysical Research Letters*
6
7 821 **47** (10): e2020GL087537
8
9
10 822 Lehner B, Liermann CR, Revenga C, Vörösmarty C, Fekete B, Crouzet P, Döll P, Endejan M,
11
12 823 Frenken K, Magome J, et al. 2011. High-resolution mapping of the world's reservoirs
13
14 824 and dams for sustainable river-flow management. *Frontiers in Ecology and the*
15
16 825 *Environment* **9** (9): 494–502
17
18
19 826 Liber Y, Mourier B, Marchand P, Bichon E, Perrodin Y, Bedell J-P. 2019. Past and recent state
20
21 827 of sediment contamination by persistent organic pollutants (POPs) in the Rhône River:
22
23 828 Overview of ecotoxicological implications. *Science of The Total Environment* **646**:
24
25 829 1037–1046
26
27
28 830 Liu K-K, Seitzinger S, Mayorga E, Harrison J, Ittekkot V. 2009. Fluxes of nutrients and selected
29
30 831 organic pollutants carried by Rivers. In *Watersheds, bays and bounded Seas: the science*
31
32 832 *and management of semi-enclosed marine systems*. Urban, E. R., Sundby, B.,
33
34 833 Malanotte-Rizzoli, P., and Melillo, J.: Island Press, Washington, DC; 141–167.
35
36
37 834 LUCRPO, LPSRIEP and Montgomery Watson 2001, Environmental Impact Assessment
38
39 835 Report for the Liao River Basin Project, Liaoning Urban Construction and Renewal
40
41 836 Project Office, Liaoning Provincial Scientific Research Institute for Environmental
42
43 837 Projection and Montgomery Watson. E430, Vol 1, viewed 17 November 2020,
44
45 838 [http://info.worldbank.org/etools/docs/library/39794/Sample-](http://info.worldbank.org/etools/docs/library/39794/Sample-EAreportLiaoRiverBasinProjectEN.pdf)
46
47 839 [EAreportLiaoRiverBasinProjectEN.pdf](http://info.worldbank.org/etools/docs/library/39794/Sample-EAreportLiaoRiverBasinProjectEN.pdf). [Accessed on 22 September 2020].
48
49
50
51 840 Ludwig W, Dumont E, Meybeck M, Heussner S. 2009. River discharges of water and nutrients
52
53 841 to the Mediterranean and Black Sea: Major drivers for ecosystem changes during past
54
55 842 and future decades? *Progress in Oceanography* **80** (3): 199–217
56
57
58 843 Macklin MG, Lewin J. 2015. The rivers of civilization. *Quaternary Science Reviews* **114**: 228–
59
60

- 1
2
3 844 244
4
5 845 Mai B, Zeng EY, Luo X, Yang Q, Zhang G, Li X, Sheng G, Fu J. 2005. Abundances,
6
7 846 depositional fluxes, and homologue patterns of polychlorinated biphenyls in dated
8
9 847 sediment cores from the Pearl River Delta, China. *Environmental Science & Technology*
10
11 848 **39** (1): 49–56
12
13
14 849 Mäkelä A, Meybeck M. 1996. Designing a monitoring programme. In *Water Quality*
15
16 850 *Monitoring: A Practical Guide to the Design and Implementation of Freshwater*
17
18 851 *Quality Studies and Monitoring Programs*, Bartram J, Ballance R (eds). London: E &
19
20 852 FN Spon; 37–59.
21
22
23 853 Malaj E, Ohe PC von der, Grote M, Kühne R, Mondy CP, Usseglio-Polatera P, Brack W,
24
25 854 Schäfer RB. 2014. Organic chemicals jeopardize the health of freshwater ecosystems
26
27 855 on the continental scale. *Proceedings of the National Academy of Sciences* **111** (26):
28
29 856 9549–9554
30
31
32
33 857 Masson M. 2007. Sources et transferts métalliques dans le bassin versant de la Gironde:
34
35 858 Réactivité et mécanismes géochimiques dans l'estuaire fluvial de la Gironde. PhD
36
37 859 Thesis, Bordeaux-I University.
38
39
40 860 Masson M, Angot H, Le Bescond C, Launay M, Dabrin A, Miège C, Le Coz J, Coquery M.
41
42 861 2018. Sampling of suspended particulate matter using particle traps in the Rhône River:
43
44 862 Relevance and representativeness for the monitoring of contaminants. *The Science of*
45
46 863 *the Total Environment* **637–638**: 538–549
47
48
49 864 McConnell JR, Chellman NJ, Wilson AI, Stohl A, Arienzo MM, Eckhardt S, Fritzsche D,
50
51 865 Kipfstuhl S, Opel T, Place PF, Steffensen JP, 2019. Pervasive Arctic lead pollution
52
53 866 suggests substantial growth in medieval silver production modulated by plague, climate,
54
55 and conflict. *PNAS* **116** (30): 14910–14915
56
57
58 868 Meybeck M. 2003. Global analysis of river systems: from Earth system controls to
59
60

- 1
2
3 869 Anthropocene syndromes. *Philosophical Transactions of the Royal Society B:*
4
5 870 *Biological Sciences* **358** (1440): 1935–1955
6
7
8 871 Meybeck M, Helmer R. 1989. The quality of rivers: From pristine stage to global pollution.
9
10 872 *Palaeogeography, Palaeoclimatology, Palaeoecology* **75** (4): 283–309
11
12 873 Miller JR, Orbock Miller SM. 2007. Contaminated rivers: a geomorphological-geochemical
13
14 874 approach to site assessment and remediation. Springer: Dordrecht, Pays-Bas. Mourier B,
15
16 875 Desmet M, Van Metre PC, Mahler BJ, Perrodin Y, Roux G, Bedell J-P, Lefèvre I, Babut
17
18 876 M. 2014. Historical records, sources, and spatial trends of PCBs along the Rhône River
19
20 877 (France). *The Science of the Total Environment* **476–477**: 568–576
21
22
23
24 878 Mouyen M, Longuevergne L, Steer P, Crave A, Lemoine J-M, Save H, Robin C. 2018.
25
26 879 Assessing modern river sediment discharge to the ocean using satellite gravimetry.
27
28 880 *Nature Communications* **9** (1): 3384
29
30
31 881 Nienhuis JH, Ashton AD, Edmonds DA, Hoitink AJF, Kettner AJ, Rowland JC, Törnqvist TE.
32
33 882 2020. Global-scale human impact on delta morphology has led to net land area gain.
34
35 883 *Nature* **577** (7791): 514–518
36
37
38 884 Nowak KC. 2011. Stochastic Streamflow Simulation at Interdecadal Times Scales and
39
40 885 Implications for Water Resources Management in the Colorado River Basin. PhD
41
42 886 Thesis, University of Colorado.
43
44
45 887 Noyes PD, McElwee MK, Miller HD, Clark BW, Van Tiem LA, Walcott KC, Erwin KN,
46
47 888 Levin ED. 2009. The toxicology of climate change: environmental contaminants in a
48
49 889 warming world. *Environment International* **35** (6): 971–986
50
51
52 890 Pacyna JM, Pacyna EG. 2001. An assessment of global and regional emissions of trace metals
53
54 891 to the atmosphere from anthropogenic sources worldwide. *Environmental Reviews:*
55
56 892 269–298
57
58
59 893 Panayotou T. 2000. Economic Growth and the Environment. *CID Working Paper Series* **56**:
60

- 1
2
3 894 119
4
5 895 Pardé M. 1925. Le régime du Rhône. *Revue de Géographie Alpine* **13** (3): 459–547 (in French).
6
7
8 896 Pettitt A.N. (1979). A non-parametric approach to the change-point problem. *Applied Statistics*
9
10 897 28, 126-135.
11
12 898 Pfeiffer WC, Lacerda LD, Salomons W, Malm O. 1993. Environmental fate of mercury from
13
14 899 gold mining in the Brazilian Amazon. *Environmental Reviews*: 26–37
15
16
17 900 Pizzuto J.E. 2014. Long-term storage and transport length scale of fine sediment: Analysis of
18
19 901 a mercury release into a river. *Geophysical Research Letters* **41** (16): 5875–5882
20
21 902 Poulhier G, Launay M, Le Bescond C, Thollet F, Coquery M, Le Coz J. 2019. Combining flux
22
23 903 monitoring and data reconstruction to establish annual budgets of suspended particulate
24
25 904 matter, mercury and PCB in the Rhône River from Lake Geneva to the Mediterranean
26
27 905 Sea. *The Science of the Total Environment* **658**: 457–473
28
29
30 906 Qi W, Müller B, Pernet-Coudrier B, Singer H, Liu H, Qu J, Berg M. 2014. Organic
31
32 907 micropollutants in the Yangtze River: Seasonal occurrence and annual loads. *Science of*
33
34 908 *The Total Environment* **472**: 789–799
35
36
37 909 Rasmussen JJ, Wiberg-Larsen P, Baattrup-Pedersen A, Monberg RJ, Kronvang B. 2012.
38
39 910 Impacts of pesticides and natural stressors on leaf litter decomposition in agricultural
40
41 911 streams. *The Science of the Total Environment* **416**: 148–155
42
43
44 912
45
46 913 Rockström J, Steffen W, Noone K, Persson A, Chapin FS, Lambin EF, Lenton TM, Scheffer
47
48 914 M, Folke C, Schellnhuber HJ, et al. 2009. A safe operating space for humanity. *Nature*
49
50 915 **461** (7263): 472–475
51
52
53 916 Roulet M, Lucotte M, Farella N, Serique G, Coelho H, Sousa Passos C, de Jesus da Silva E,
54
55 917 Scavone de Andrade P, Mergler D, Guimarães J-RD, et al. 1999. Effects of Recent
56
57 918 Human Colonization on the Presence of Mercury in Amazonian Ecosystems |
58
59
60

- 1
2
3 919 SpringerLink. *Water, Air, and Soil Pollution* **112**: 297–313
4
5 920 Rügner H, Schwientek M, Milačić R, Zuliani T, Vidmar J, Paunović M, Laschou S,
6
7 921 Kalogianni E, Skoulikidis NT, Diamantini E, et al. 2019. Particle bound pollutants in
8
9 922 rivers: Results from suspended sediment sampling in Globaqua River Basins. *The*
10
11 923 *Science of the Total Environment* **647**: 645–652
12
13 924 Sartorius C, Hillenbrand T, Walz R. 2011. Impact and cost of measures to reduce nutrient
14
15 925 emissions from wastewater and storm water treatment in the German Elbe river basin.
16
17 926 *Regional Environmental Change* **11**: 377–391
18
19 927 Schäfer RB, Gerner N, Kefford BJ, Rasmussen JJ, Beketov MA, de Zwart D, Liess M, von
20
21 928 der Ohe PC. 2013. How to characterize chemical exposure to predict ecologic effects
22
23 929 on aquatic communities? *Environmental Science & Technology* **47** (14): 7996–8004
24
25 930 Scheurle C, Hebbeln D, Jones P. 2005. An 800-year reconstruction of Elbe River discharge and
26
27 931 German Bight sea-surface salinity. *The Holocene* **15** (3): 429–434
28
29 932 Schulze T, Ricking M, Schröter-Kermani C, Körner A, Denner H-D, Weinfurtner K, Winkler
30
31 933 A, Pekdeger A. 2007. The German Environmental Specimen Bank. *Journal of Soils and*
32
33 934 *Sediments* **7** (6): 361–367
34
35 935 Schwarzenbach RP, Egli T, Hofstetter TB, von Gunten U, Wehrli B. 2010. Global Water
36
37 936 Pollution and Human Health. *Annual Review of Environment and Resources* **35** (1):
38
39 937 109–136
40
41 938 Schwarzenbach RP, Escher BI, Fenner K, Hofstetter TB, Johnson CA, Gunten U von, Wehrli
42
43 939 B. 2006. The Challenge of Micropollutants in Aquatic Systems. *Science* **313** (5790):
44
45 940 1072–1077
46
47 941 Schwientek M, Rügner H, Beckingham B, Kuch B, Grathwohl P. 2013. Integrated monitoring
48
49 942 of particle associated transport of PAHs in contrasting catchments. *Environmental*
50
51 943 *Pollution* **172**: 155–162
52
53
54
55
56
57
58
59
60

- 1
2
3 944 Shafik N. 1994. Economic Development and Environmental Quality: An Econometric
4
5 945 Analysis. *Oxford Economic Papers* **46** (Special Issue on Environmental Economics):
6
7 946 757–773
- 9
10 947 Shafik, N., Bandyopadhyay, S. 1992. Economic Growth and Environmental Quality: Time-
11
12 948 Series and Cross-Country Evidence. Background Paper for the World Development
13
14 949 Report. The World Bank, Washington, DC.
- 16
17 950 Shen H, Huang Y, Wang R, Zhu D, Li W, Shen G, Wang B, Zhang Y, Chen Y, Lu Y, et al.
18
19 951 2013. Global atmospheric emissions of polycyclic aromatic hydrocarbons from 1960 to
20
21 952 2008 and future predictions. *Environmental science & technology* **47** (12): 6415–6424
- 23
24 953 Shen H, Tao S, Wang R, Wang B, Shen G, Li W, Su S, Huang Y, Wang X, Liu W, et al. 2011.
25
26 954 Global time trends in PAH emissions from motor vehicles. *Atmospheric Environment*
27
28 955 **45** (12): 2067–2073
- 30
31 956 Singer MB, Aalto R, James LA, Kilham NE, Higson JL, Ghoshal S. 2013. Enduring legacy of
32
33 957 a toxic fan via episodic redistribution of California gold mining debris. *Proceedings of*
34
35 958 *the National Academy of Sciences* **110** (46): 18436–18441
- 37
38 959 Steffen W, Richardson K, Rockström J, Cornell SE, Fetzer I, Bennett EM, Biggs R, Carpenter
39
40 960 SR, de Vries W, de Wit CA, et al. 2015. Sustainability. Planetary boundaries: guiding
41
42 961 human development on a changing planet. *Science* **347** (6223): 736–746
- 44
45 962 Stern DI. 2004. The Rise and Fall of the Environmental Kuznets Curve. *World Development*
46
47 963 **32** (8): 1419–1439
- 48
49 964 Stern DI, Common MS, Barbier EB. 1996. Economic growth and environmental degradation:
50
51 965 The environmental Kuznets curve and sustainable development. *World Development* **24**
52
53 966 (7): 1151–1160
- 55
56 967 Stigliani WM. 1991. Chemical Time Bombs: Definition, Concepts, and Examples. Executive
57
58 968 report 16. International institute for applied systems analysis, Laxenburg, Austria.
- 60

- 1
2
3 969 Streets DG, Horowitz HM, Jacob DJ, Lu Z, Levin L, ter Schure AFH, Sunderland EM. 2017.
4
5 970 Total Mercury Released to the Environment by Human Activities. *Environmental*
6
7 971 *Science & Technology* **51** (11): 5969–5977
- 9
10 972 Sutfin NA, Wohl E. 2019. Elevational differences in hydrogeomorphic disturbance regime
11
12 973 influence sediment residence times within mountain river corridors. *Nature*
13
14 974 *Communications* **10** (1): 2221
- 16
17 975 Syvitski JPM, Kettner AJ. 2007. On the flux of water and sediment into the Northern Adriatic
18
19 976 Sea. *Continental Shelf Research* **27** (3): 296–308
- 21
22 977 Syvitski JPM, Vörösmarty CJ, Kettner AJ, Green P. 2005. Impact of humans on the flux of
23
24 978 terrestrial sediment to the global coastal ocean. *Science* **308** (5720): 376–380
- 26
27 979 Syvitski PM, Kettner A. 2011. Sediment flux and the Anthropocene. *Philosophical*
28
29 980 *Transactions of the Royal Society A: Mathematical, Physical and Engineering Sciences*
30
31 981 **369** (1938): 957–975
- 33
34 982 Thollet F, Le Bescond C, Lagouy M, Gruat A, Grisot G, Le Coz J, Coquery M, Lepage H,
35
36 983 Gairoard S, Gattacceca JC, Ambrosi J-P, Radakovitch O, Dur G, Richard L, Giner F,
37
38 984 Eyrolle F, Angot H, Mourier D, Bonnefoy A, Dugué V, Launay M, Troudet L, Labille
39
40 985 J, Kieffer L, 2021. Observatoire des Sédiments du Rhône. Irstea. Available at:
41
42 986 <https://dx.doi.org/10.17180/OBS.OSR>
- 44
45 987 UNECE — United Nations Economic Commission for Europe. 1979 — European Environment
46
47 988 Agency. The Geneva Convention on Long-range Transboundary Air Pollution. Nations
48
49 989 Unies. Commission économique pour l'Europe, New-York. Available at:
50
51 990 [https://www.eea.europa.eu/data-and-maps/indicators/main-anthropogenic-air-](https://www.eea.europa.eu/data-and-maps/indicators/main-anthropogenic-air-pollutant-emissions/unece-1979)
52
53 991 [pollutant-emissions/unece-1979](https://www.eea.europa.eu/data-and-maps/indicators/main-anthropogenic-air-pollutant-emissions/unece-1979) [Accessed on 20 November 2020]
- 55
56 992 UNEP — United Nations Environment Programme. 2001. Final Act of the Plenipotentiaries on
57
58 993 the Stockholm Convention on Persistent Organic Pollutants. United Nations
59
60

- 1
2
3 994 Environment Program Chemicals, Geneva, Switzerland.
4
5 995 UNEP/MAP — United Nations Environment Programme — Mediterranean Action Plan.
6
7 996 2003. Riverine transport of water, sediments and pollutants to the Mediterranean Sea.
8
9 997 Technical Reports 141. Athens.
10
11 998 UNEP-DHI and UNEP — 2016. Transboundary River Basins: Status and Trends. United
12
13 999 Nations Environment Programme (UNEP). Vol. 3: River basins, Nairobi.
14
15 1000 UNESCO (ed.). 2009. *Water in a changing world*. UNESCO: Paris, London.
16
17 1001 United Nations, 1998. Protocol to the 1979 convention on long-range transboundary air
18
19 1002 pollution on persistent organic pollutants. ECE/EB.AIR/ 60.
20
21 1003 Vianello A. 2015. *Rivers in Prehistory*. Archaeopress.
22
23 1004 Wang J-Z, Guan Y-F, Ni H-G, Luo X-L, Zeng EY. 2007. Polycyclic Aromatic Hydrocarbons
24
25 1005 in Riverine Runoff of the Pearl River Delta (China): Concentrations, Fluxes, and Fate.
26
27 1006 *Environmental Science & Technology* **41** (16): 5614–5619
28
29 1007 Wilkinson P, Smith KR, Bevers S, Tonne C, Oreszczyn T. 2007. Energy, energy efficiency,
30
31 1008 and the built environment. *Lancet (London, England)* **370** (9593): 1175–1187
32
33 1009 Wohl E. 2015. Legacy effects on sediments in river corridors. *Earth-Science Reviews* **147**:
34
35 1010 30–53
36
37 1011 Wohl E. 2019. Forgotten Legacies: Understanding and Mitigating Historical Human
38
39 1012 Alterations of River Corridors. *Water Resources Research* **55** (7): 5181–5201
40
41 1013 World Bank national accounts data, and OECD National Accounts data files.
42
43 1014 <https://data.worldbank.org/indicator/NY.GDP.MKTP.CD> [Accessed on 10 October
44
45 1015 2020].
46
47 1016 World Cities Database. 2020. Creative Commons Attribution 4.0 license. Available at:
48
49 1017 <https://simplemaps.com/data/world-cities> [Accessed on 10 October 2020].
50
51 1018 Xing Y, Lu Y, Liu W. 2011. Environmental Contamination Status of Polychlorinated
52
53
54
55
56
57
58
59
60

1
2
3 1019 Biphenyls in China. In *Global Environmental Distribution and Human Health Effects*
4
5 1020 *of Polycyclic Aromatic Hydrocarbons*, Loganathan BG, Lam PKS (eds). CRC Press:
6
7 1021 Boca Raton (FL, USA); 163–177.

8
9
10 1022 Xu S, Jiang X, Dong Y, Sun C, Feng J, Wang L, Martens D, Gawlik BM. 2000. Polychlorinated
11
12 1023 organic compounds in Yangtze River sediments. *Chemosphere* **41** (12): 1897–1903

13
14
15 1024

16 1025 **Captions of the figures and tables**

17
18 1026 **Figure 1.** (A) Map of the Rhône River basin with its main tributaries and monitoring stations
19
20 1027 for water discharge, suspended particulate matter, and associated micropollutants. (B) Land-
21
22 1028 use distribution (in %) in the basin of the Rhône River (Arles/Beaucaire station) and its main
23
24 1029 tributaries.

25
26
27 1030 **Figure 2.** Changes of $\sum_7\text{PCBi}$ (A and B), $\sum_{12}\text{PAH}$ (C and D) and TME (E and F) concentrations
28
29 1031 (μg or mg kg^{-1}) and fluxes (kg or t yr^{-1}) since the 1980s at the Rhône River outlet. The high-
30
31 1032 resolution temporal trend of micropollutant concentrations over the 2000–2010 period is
32
33 1033 detailed in Fig. 3. In panels A and B, the black arrow labeled “1975” indicates the year that
34
35 1034 PCBs were banned in closed devices (order of 8 July 1975), and the black arrow labeled “1987”
36
37 1035 indicates the year of the blanket ban on the same PCBs and the ban on the production of devices
38
39 1036 using PCBs at $> 0.5 \text{ g kg}^{-1}$ (decree 87-59).

40
41
42
43 1037 **Figure 3.** High-resolution temporal trend of $\sum_7\text{PCBi}$, $\sum_{12}\text{PAH}$ and TME concentrations (μg or
44
45 1038 mg kg^{-1}) from 2008 to 2019 at the Rhône River mouth (Arles/Beaucaire station). Blue
46
47 1039 histograms show mean monthly water discharges ($\text{m}^3 \text{ s}^{-1}$) at the Rhône River outlet. Red dotted
48
49 1040 lines show the temporal trends in micropollutant concentration time-series (see § 4.1.1. for
50
51 1041 statistical treatment details); and red values indicate increasing or decreasing contamination
52
53 1042 rates (μg or $\text{mg kg}^{-1} \text{ yr}^{-1}$), respectively, over the total length of the time-series. Green dotted
54
55 1043 lines indicate the trend change-point dates (see § 4.1.1. for statistical treatment details); and the
56
57 1044 green values indicate increasing or decreasing contamination rates before and after the change-

1
2
3 1045 point dates (μg or $\text{mg kg}^{-1} \text{yr}^{-1}$). Only the temporally significant trends are shown (p -value <
4
5 1046 0.05 for non-parametric Mann-Kendall tests).

7 1047 **Figure 4.** Maps of the $\sum_{12}\text{PAH}$, $\sum_5\text{PCBi}$, TME and SPM yields in the Rhône River basin and
9
10 1048 its main sub-basins.

12 1049 **Figure 5.** Principal Component Analysis (PCA) of all inter-annual micropollutant yields, land-
13
14 use cover and population density for the monitoring stations on the Rhône River basin and at
15 1050 its outlet (Arles/Beaucaire station). See Supporting Text for details on PCA method used. The
16
17 1051 land-use classification used is the same as for Fig. 1B, i.e. “Agri” for agricultural lands,
18
19 1052 “Forests” for forest areas, “Bare” for bare areas, “Vegetal” for shrub and/or grassy vegetation,
20
21 1053 “ICA” for industrial and commercial areas, and “Urban” for urban areas. On the whole, the
22
23 1054 dominant factor F1 results from the contribution of all micropollutant (except for $\sum_5\text{PCBi}$) and
24
25 1055 SPM yields. Factor F2 opposes the anthropogenic-related land use categories (urban,
26
27 1056 agricultural, industrial and commercial areas) against the forests land-use category.
28
29 1057

32
33 1058 **Figure 6.** Maps of the $\sum_{12-16}\text{PAH}$, $\sum_7\text{PCBi}$, Hg, Cd and SPM yields, and GDP per capita in the
34
35 1059 major world river basins (1-Rhône, 2-Garonne, 3-Loire, 4-Seine, 5-Volga, 6-Danube, 7-Elbe,
36
37 1060 8-Rhine, 9-Pearl (Zhujiang), 10-Liao, 11-Yangtze (Changjiang), 12-Yellow (Huang He), 13-
38
39 1061 Mekong, 14-Ganges-Brahmaputra, 15-Mississippi, 16-Colorado, 17-St. Lawrence, 18-
40
41 1062 Amazon, 19-Niger).

44 1063 **Figure 7.** PCA of all micropollutant and SPM yields, density of dams, populations and cities,
45
46 1064 and GDP per capita in the major world river basins (see Supporting Text for details on the
47
48 1065 PCA). On the whole, the dominant factor F1 results from the contribution of a large share of
49
50 1066 micropollutant and SPM yields, and factor F2 is mostly driven by economic parameters (dams
51
52 1067 density, population density, cities density, and GDP per capita). Panel A shows the correlation
53
54 1068 circle in which three groups of micropollutant yields gather (gray ellipses) according to their
55
56 1069 correlations with SPM yields and median micropollutant concentrations (Fig. S2) (see
57
58
59
60

1
2
3 1070 correlation coefficients and p-values in text and Tab. S3 and S4). Thus, groups 1, 2 and 3 are
4
5 1071 anthropogenic activity-driven micropollutant yields, SPM flux-driven micropollutant yields
6
7
8 1072 and anthropogenic activity/SPM flux-driven micropollutant yields, respectively. Panel B
9
10 1073 displays the observations plot defining three mixing lines (gray dotted lines) for overall
11
12 1074 contamination level from the least-contaminated river basins in the bottom-left corner of the
13
14 1075 graph up to the most-contaminated river basins in the upper-right part of the graph. Mixing
15
16 1076 lines were statistically defined as follows: linking the origin to the average F1 and F2 biplot
17
18 1077 loadings (gray crosses) across all 11 micropollutants (Groups 1 + 2 + 3-based mixing line), a
19
20 1078 set of 7 micropollutants (Groups 1 + 3-based mixing line) and a set of 4 micropollutants (Group
21
22 1079 1-based mixing line). Slope angularity of the mixing lines thus gives the balance between the
23
24 1080 anthropogenic origin of the micropollutant yields (Group 1-based mixing line) and the weight
25
26 1081 of the SPM fluxes in the micropollutant yields (Groups 1 + 2 + 3-based mixing line). The black
27
28 1082 curved arrow shows the environmental quality improvement of the Rhône River basin since the
29
30 1083 1980s.

31
32
33
34
35
36 1084 **Figure 8.** Inter-annual micropollutant yields of the major river basins (Rhône, Garonne, Loire,
37
38 1085 Seine, Volga, Danube, Elbe, Rhine, Pearl (Zhujiang), Liao, Yangtze (Changjiang), Yellow
39
40 1086 (Huang He), Mekong, Ganges-Brahmaputra, Mississippi, Colorado, St. Lawrence, Amazon and
41
42 1087 Niger Rivers).

43
44
45 1088 **Table 1.** Main physical and human characteristics of the large river basins investigated in this
46
47 1089 study. Data sources are shown in footnotes.

48
49
50 1090 **Table 2.** River sediment matrices and data sources used to assess the temporal trends in
51
52 1091 particulate micropollutant concentrations and fluxes at the Rhône River outlet listed by
53
54 1092 micropollutant family and the decades considered.

1
2
3 1093 **Table 3.** Long-term decadal variations (in %) in inter-annual particulate micropollutant
4
5 1094 concentrations (ΔC) and fluxes (ΔF) and SPM fluxes at the Rhône River outlet. Orange cells
6
7 1095 show the micropollutant flux variations that are mainly dependent on micropollutant
8
9 1096 concentration variations, while grey cells highlight micropollutant flux variations that are
10
11 1097 mainly dependent on SPM flux variations. The bottom part of the table shows the correlation
12
13 1098 coefficients for decadal micropollutant fluxes and concentrations (first line) and for
14
15 1099 micropollutant fluxes and SPM fluxes (second line).
16
17
18
19
20
21
22
23
24
25
26
27
28
29
30
31
32
33
34
35
36
37
38
39
40
41
42
43
44
45
46
47
48
49
50
51
52
53
54
55
56
57
58
59
60

For Peer Review

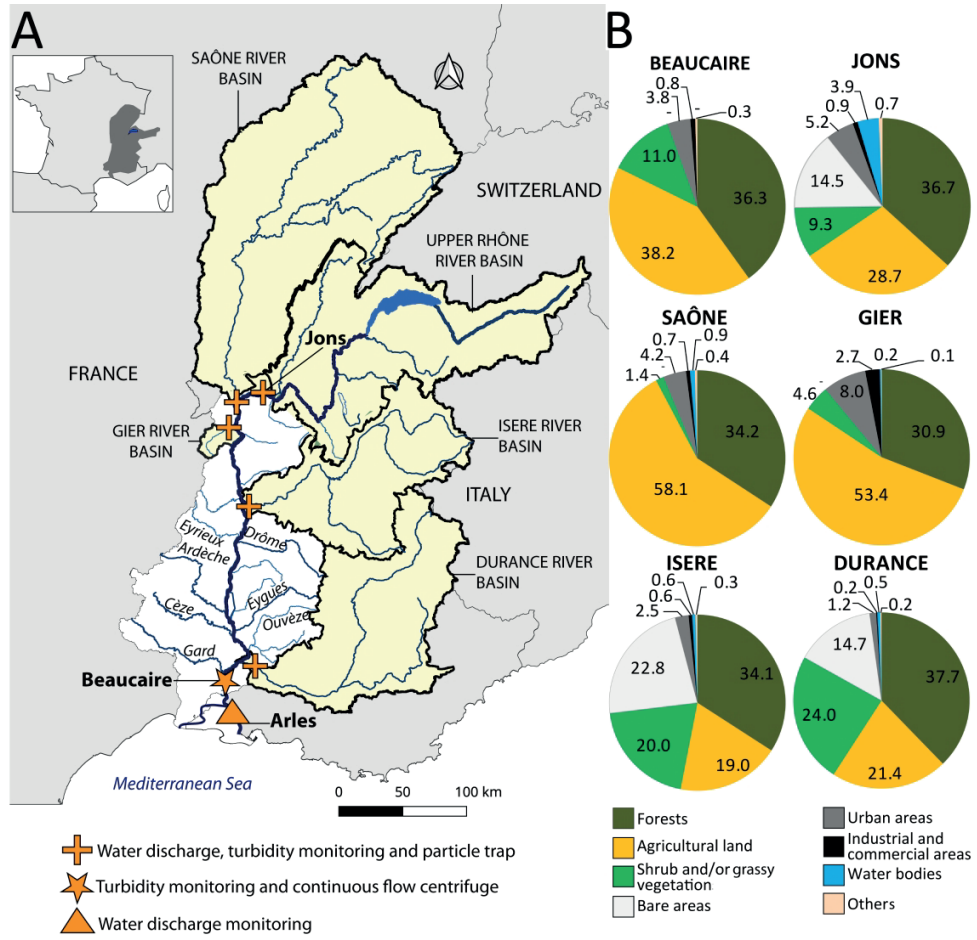


Figure 1. (A) Map of the Rhône River basin with its main tributaries and monitoring stations for water discharge, suspended particulate matter, and associated micropollutants. (B) Land-use distribution (in %) in the basin of the Rhône River (Arles/Beaucaire station) and its main tributaries.

299x288mm (400 x 400 DPI)

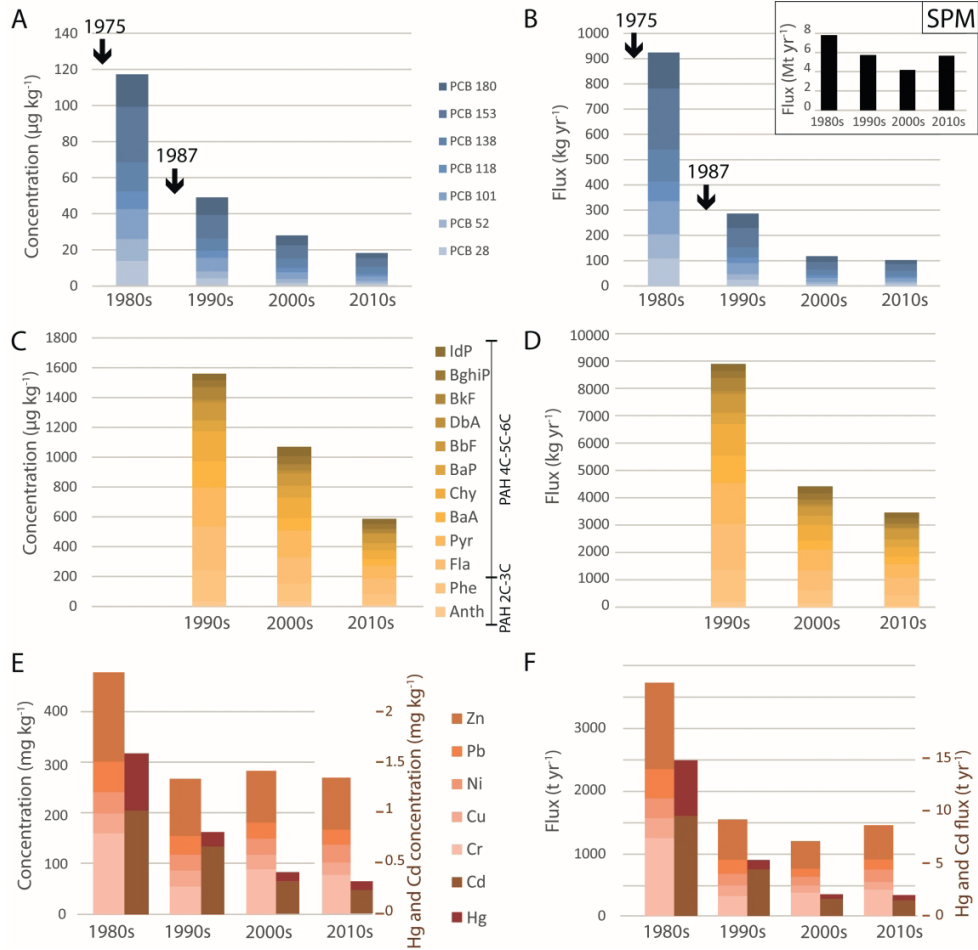


Figure 2. Changes of $\Sigma 7\text{PCBi}$ (A and B), $\Sigma 12\text{PAH}$ (C and D) and TME (E and F) concentrations (μg or mg kg^{-1}) and \rightarrow fluxes (kg or t yr^{-1}) since the 1980s at the Rhône River outlet. The high-resolution temporal trend of micropollutant concentrations over the 2000–2010 period is detailed in Fig. 3. In panels A and B, the black arrow labeled “1975” indicates the year that PCBs were banned in closed devices (order of 8 July 1975), and the black arrow labeled “1987” indicates the year of the blanket ban on the same PCBs and the ban on the production of devices using PCBs at $> 0.5 \text{ g kg}^{-1}$ (decree 87-59).

196x191mm (600 x 600 DPI)

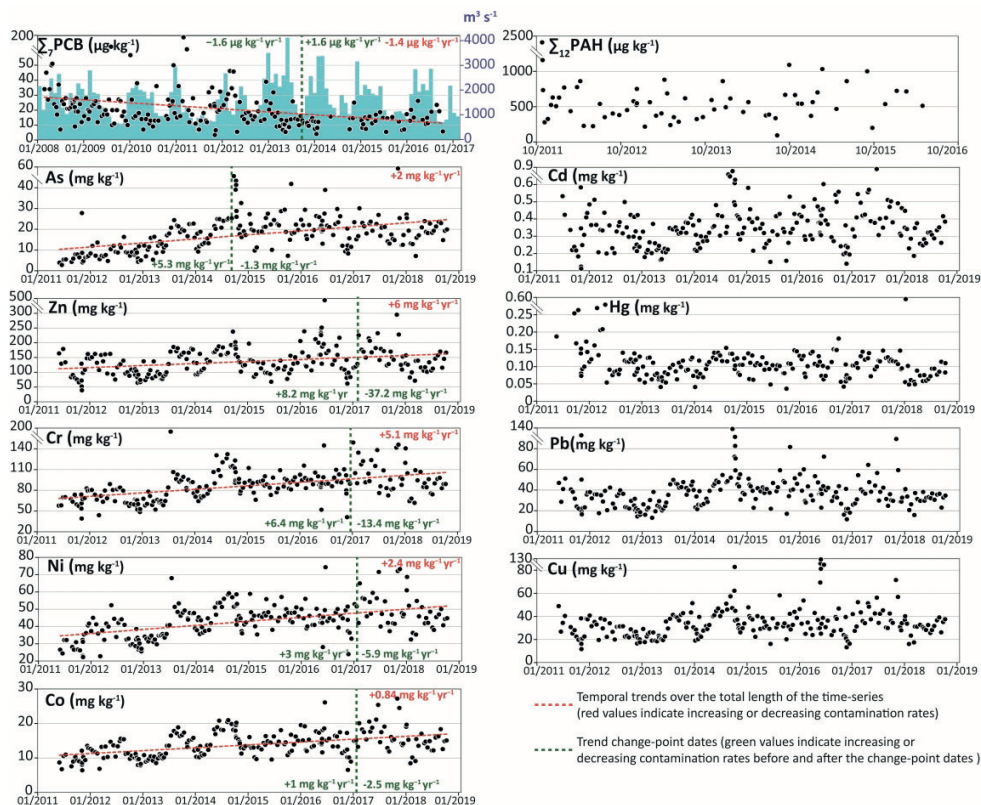


Figure 3. High-resolution temporal trend of $\Sigma 7\text{PCBi}$, $\Sigma 12\text{PAH}$ and TME concentrations (μg or mg kg^{-1}) from 2008 to 2019 at the Rhône River mouth (Arles/Beaucaire station). Blue histograms show mean monthly water discharges ($\text{m}^3 \text{s}^{-1}$) at the Rhône River outlet. Red dotted lines show the temporal trends in micropollutant concentration time-series (see § 4.1.1. for statistical treatment details); and red values indicate increasing or decreasing contamination rates (μg or $\text{mg kg}^{-1} \text{yr}^{-1}$), respectively, over the total length of the time-series. Green dotted lines indicate the trend change-point dates (see § 4.1.1. for statistical treatment details); and the green values indicate increasing or decreasing contamination rates before and after the change-point dates (μg or $\text{mg kg}^{-1} \text{yr}^{-1}$). Only the temporally significant trends are shown ($p\text{-value} < 0.05$ for non-parametric Mann-Kendall tests).

402x332mm (400 x 400 DPI)

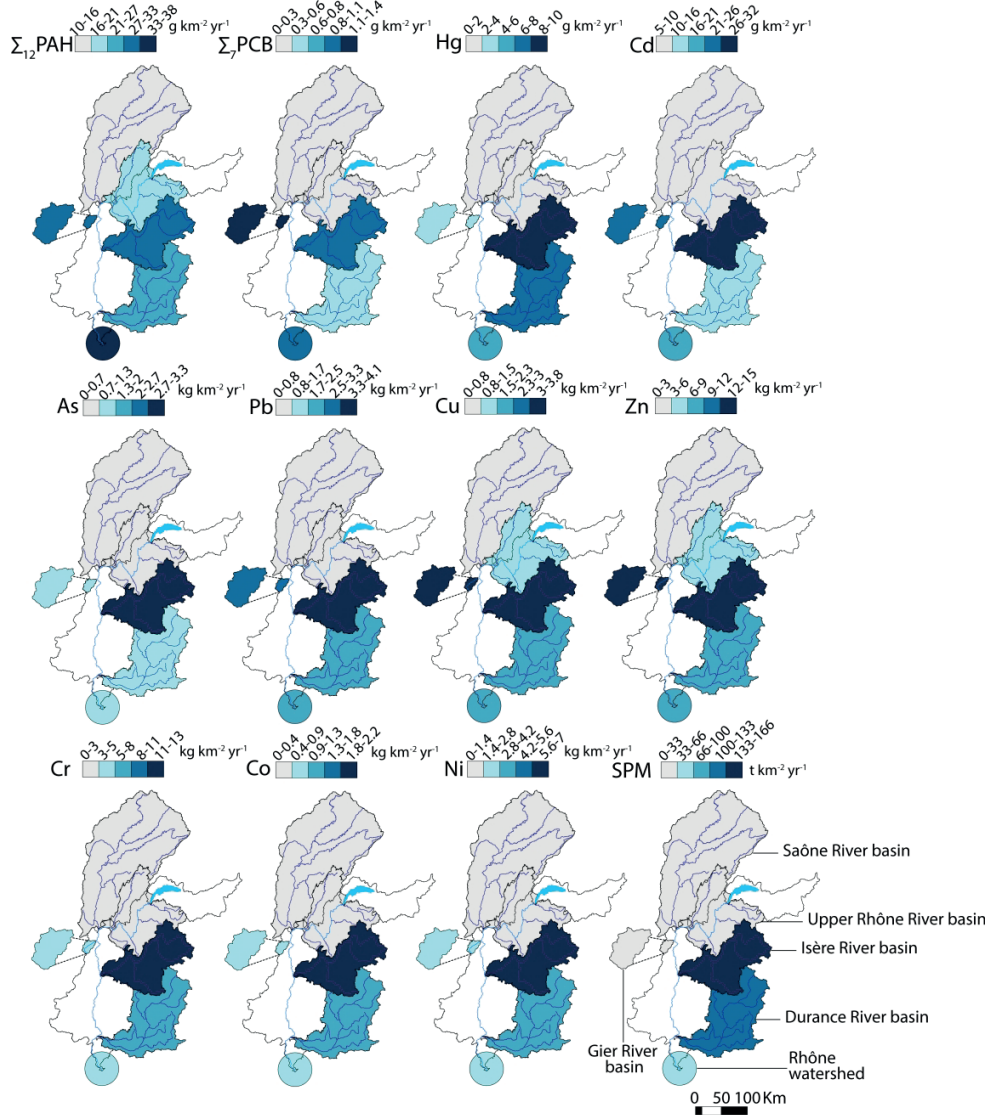


Figure 4. Maps of the $\Sigma_{12}\text{PAH}$, $\Sigma_5\text{PCB}$, TME and SPM yields in the Rhône River basin and its main sub-basins.

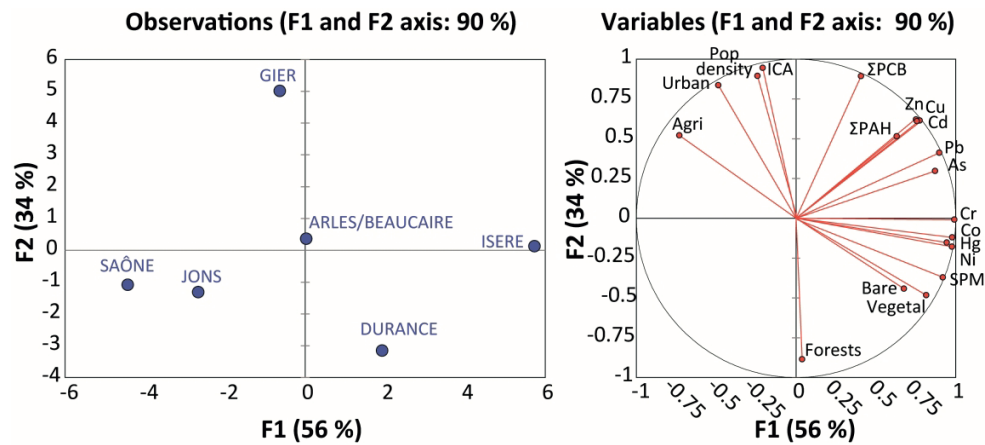


Figure 5. Principal Component Analysis (PCA) of all inter-annual micropollutant yields, land-use cover and population density for the monitoring stations on the Rhône River basin and at its outlet (Arles/Beaucaire station). See Supporting Text for details on PCA method used. The land-use classification used is the same as for Fig. 1B, i.e. "Agri" for agricultural lands, "Forests" for forest areas, "Bare" for bare areas, "Vegetal" for shrub and/or grassy vegetation, "ICA" for industrial and commercial areas, and "Urban" for urban areas. On the whole, the dominant factor F1 results from the contribution of all micropollutant (except for Σ 5PCBi) and SPM yields. Factor F2 opposes the anthropogenic-related land use categories (urban, agricultural, industrial and commercial areas) against the forests land-use category.

178x80mm (600 x 600 DPI)

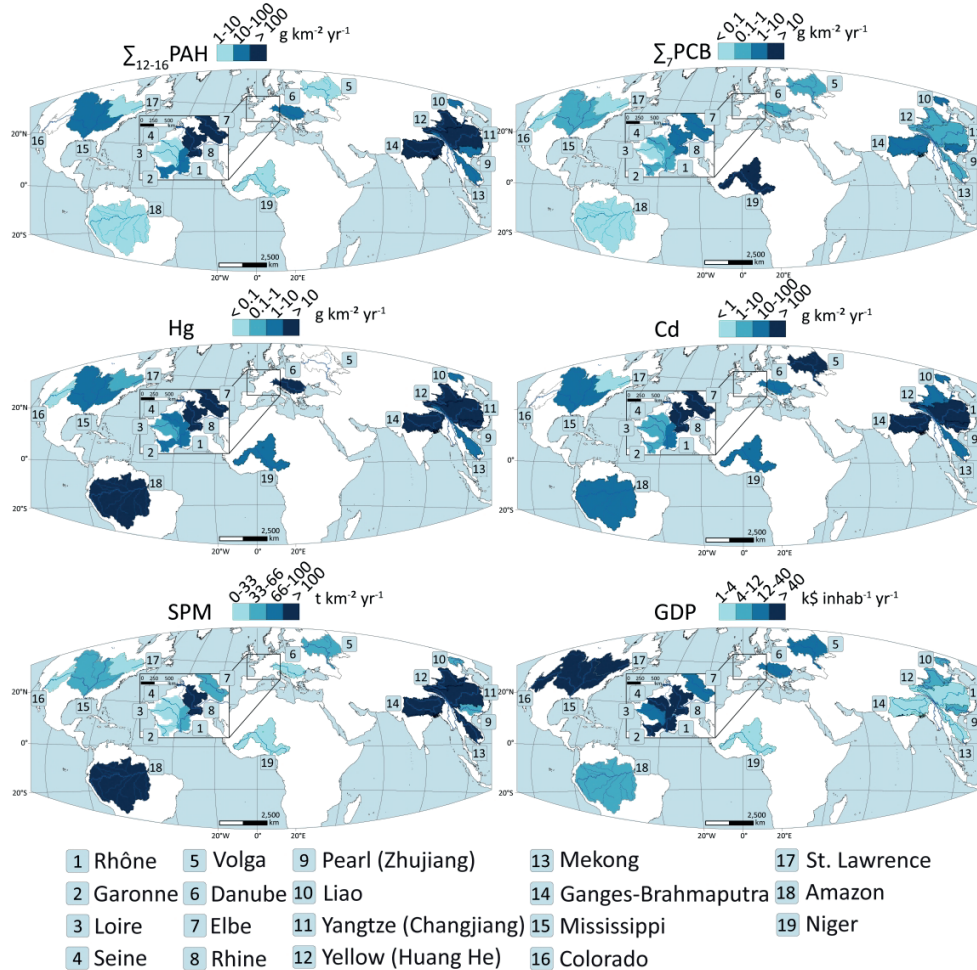


Figure 6. Maps of the $\Sigma_{12-16}\text{PAH}$, $\Sigma_7\text{PCB}$, Hg, Cd and SPM yields, and GDP per capita in the major world river basins (1-Rhône, 2-Garonne, 3-Loire, 4-Seine, 5-Volga, 6-Danube, 7-Elbe, 8-Rhine, 9-Pearl (Zhujiang), 10-Liao, 11-Yangtze (Changjiang), 12-Yellow (Huang He), 13-Mekong, 14-Ganges-Brahmaputra, 15-Mississippi, 16-Colorado, 17-St. Lawrence, 18-Amazon, 19-Niger).

424x425mm (350 x 350 DPI)

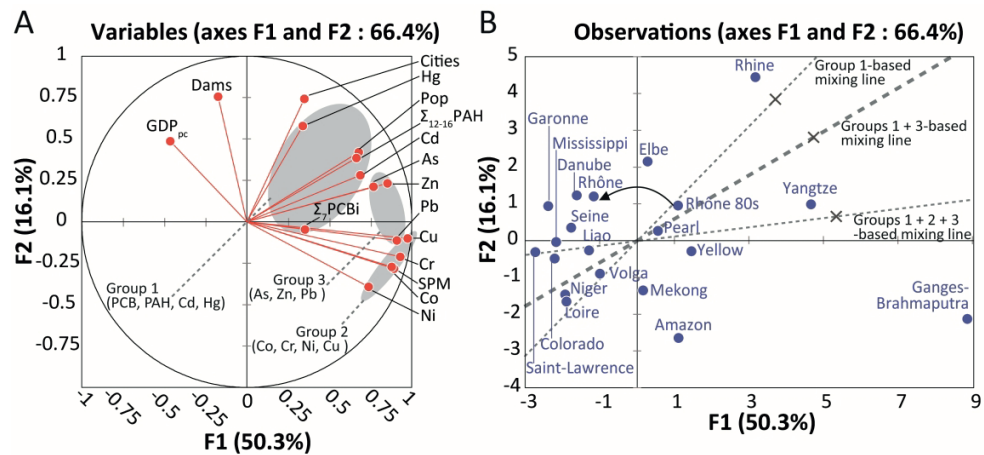


Figure 7. PCA of all micropollutant and SPM yields, density of dams, populations and cities, and GDP per capita in the major world river basins (see Supporting Text for details on the PCA). On the whole, the dominant factor F1 results from the contribution of a large share of micropollutant and SPM yields, and factor F2 is mostly driven by economic parameters (dams density, population density, cities density, and GDP per capita). Panel A shows the correlation circle in which three groups of micropollutant yields gather (gray ellipses) according to their correlations with SPM yields and median micropollutant concentrations (Fig. S2) (see correlation coefficients and p-values in text and Tab. S3 and S4). Thus, groups 1, 2 and 3 are anthropogenic activity-driven micropollutant yields, SPM flux-driven micropollutant yields and anthropogenic activity/SPM flux-driven micropollutant yields, respectively. Panel B displays the observations plot defining three mixing lines (gray dotted lines) for overall contamination level from the least-contaminated river basins in the bottom-left corner of the graph up to the most-contaminated river basins in the upper-right part of the graph. Mixing lines were statistically defined as follows: linking the origin to the average F1 and F2 biplot loadings (gray crosses) across all 11 micropollutants (Groups 1 + 2 + 3-based mixing line), a set of 7 micropollutants (Groups 1 + 3-based mixing line) and a set of 4 micropollutants (Group 1-based mixing line). Slope angularity of the mixing lines thus gives the balance between the anthropogenic origin of the micropollutant yields (Group 1-based mixing line) and the weight of the SPM fluxes in the micropollutant yields (Groups 1 + 2 + 3-based mixing line). The black curved arrow shows the environmental quality improvement of the Rhône River basin since the 1980s.

192x89mm (600 x 600 DPI)

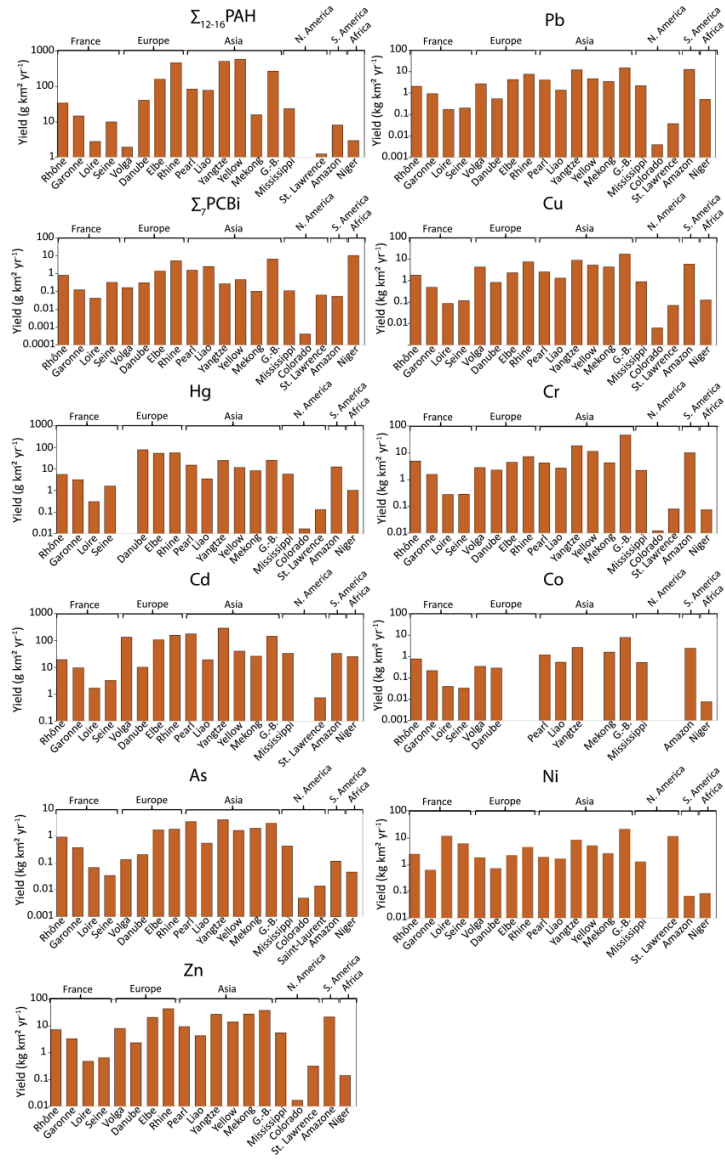


Figure 8. Inter-annual micropollutant yields of the major river basins (Rhône, Garonne, Loire, Seine, Volga, Danube, Elbe, Rhine, Pearl (Zhujiang), Liao, Yangtze (Changjiang), Yellow (Huang He), Mekong, Ganges-Brahmaputra, Mississippi, Colorado, St. Lawrence, Amazon and Niger Rivers).

1223x1979mm (96 x 96 DPI)

	Lenght (km)	Watershed (km ²)	Mean water discharge (m ³ s ⁻¹)	SPM flux (Mt yr ⁻¹)	SPM yield (t km ⁻² yr ⁻¹)	Population (M inhab)	Population density (inhab km ²)	Number of large cities (> 500 000)	Cities density (cities 10 ⁵ km ²)	GDP (billion USD yr ⁻¹)	GDP per capita (USD yr ⁻¹)	Number of dams	Dams density (M km ²)
1	765 ¹	89 000 ²	1 620 ³	5.5 ³	63	15.5 ⁴	175	12 ²	14	642	41 421 ²	30 ²	337
2	529 ⁵	51 257 ⁵	650 ⁵	1 ⁵	20	5.9 ⁵	115	2 ²	4	244	41 421 ²	24 ²	427
3	1006 ⁵	110 726 ⁵	870 ⁵	0.4 ⁵	3.8	14.3 ⁵	129	2 ⁶	2	451	31 555 ⁶	3 ⁵	27
4	775 ⁵	65 366 ⁵	600 ⁵	0.4 ⁵	6.5	20.1 ⁵	307	7 ²	11	833	41 421 ²	10 ²	136
5	3 692 ⁷	1 411 000 ²	8 103 ⁷	47.3 ⁸	33.5	58.6 ²	42	74 ²	5	857	14 612 ²	17 ²	12
6	2 900 ⁷	796 000 ²	6 659 ⁷	20.2 ⁸	25.4	80.2 ²	101	63 ²	8	1 482	18 478 ²	184 ²	231
7	1 165 ¹⁰	148 268 ⁹	750 ¹⁰	7.9 ⁸	53.2	24.7 ⁹	167	16 ²	11	937	37 940 ²	42 ²	302
8	1 400 ⁷	163 609 ²	2 347 ⁷	17.3 ⁸	105.8	48.8 ²	298	62 ²	38	2 419	49 543 ²	42 ²	257
9	2 200 ⁷	490 000 ⁷	8 245 ⁷	25 ⁸	51	75 ⁷	153	40 ²	8	506	6 740 ²	49 ²	122
10	1 345 ¹²	229 000 ¹²	82 ¹²	9 ¹²	39.3	33 ¹¹	144	20 ¹³	9	156 ¹³	4 716	41 ¹⁴	179
11	6 300 ⁷	1 800 000 ⁷	28 538 ⁷	284 ⁸	157	601 ¹⁵	332	56 ¹³	3	1 796 ¹³	2 988	380 ¹⁴	210
12	5 500 ⁷	750 000 ⁷	1 364 ⁷	120 ⁸	159	162 ¹⁵	215	36 ¹³	5	751 ¹³	4 636	48 ¹⁴	64
13	4 800 ⁷	773 000 ⁷	17 440 ⁷	95 ⁸	122	59 ²	76	16 ²	2	226	3854 ²	20 ²	26
14	5 900 ⁷	3 208 000 ⁷	15 538 ⁷	132 ⁸	41	78.2 ²	24	54 ²	1.7	4 154	53 142 ²	707 ²	220
15	2 330 ¹⁶	626 050 ²	640 ¹⁷	0.13 ⁸	0.2	8.8 ²	14	16 ²	2.5	456	51 802 ²	82 ²	131
16	4 000 ⁷	1 057 304 ⁷	10 781 ⁷	4.6 ⁸	4.4	45.9 ²	43	37 ²	3.5	2 416	52 663 ²	176 ²	166
17	4 000 ⁷	2 111 475 ⁷	6 025 ⁷	25.2 ⁸	11.9	93.6 ⁷	44	33 ²	1.6	199	2 125 ²	56 ²	27
18	6 300 ⁷	5 888 269 ²	199 772 ⁷	978 ⁸	166	32.2 ²	5.5	21 ²	0.4	225	6 998 ²	8 ²	1
19	2 600 ⁷	1 652 367 ²	17 760 ⁷	1 104 ⁸	669	540.4 ⁷	327	194 ²	12	728	1 347 ²	82 ²	50

¹⁷Nowak (2011)¹³World Bank⁹Sartorius & Hillenbrand (2011)⁵Dendrievel et al. (2020b)¹Bravard & Clémens (2018)¹⁰Scheurle et al. (2005)⁶INSEE²UNEP-DHI & UNEP (2016)¹¹LUCRPO et al. (2001)⁷Best (2019)³Delile et al. (2020)¹²Liu et al. (2013)⁸Nienhuis et al. (2020)⁴AERMC (2019)¹⁴Lehner et al. (2011)¹⁵Immerzeel & Bierkens (2012)¹⁶Kammerer (1990)

Micropollutants family	Studied periods	River sediment matrices	Data sources	References and availability
TME (Cd, Cr, Cu, Hg, Ni, Pb, Zn)	1980s-2010s	Bed and flood deposits, sediment cores, and SPM	Rhône–Mediterranean–Corsica water agency, OSR monitoring program, and research institutes	Dendievel et al., 2020a,b; Thollet et al., 2021; Delile et al., 2020.
TME (As, Cd, Co, Cr, Cu, Hg, Ni, Pb and Zn)	2011-2018	SPM	OSR monitoring program	Thollet et al., 2021; Delile et al., 2020.
PCBi (congeners 28, 52, 101, 118, 138, 153, and 180)	1980s-2010s	Bed and flood deposits, sediment cores, and SPM	Rhône–Mediterranean–Corsica water agency, OSR monitoring program, and research labs	Dendievel et al., 2020a,b; Thollet et al., 2021; Delile et al., 2020.
PCBi (congeners 28, 52, 101, 118, 138, 153, and 180)	2008-2017	SPM	OSR monitoring program	Thollet et al., 2021; Delile et al., 2020.
PAHs (Ant, BaA, BaP, BbF, BghiP, BkF, Chy, DbA, Fla, IdP, Phe, Pyr)	1990s-2010s	Bed and flood sediments , and SPM	Rhône–Mediterranean–Corsica water agency, OSR monitoring program	http://www.naiades.ea.ufrance.fr; Thollet et al., 2021; Delile et al., 2020.
PAHs (Ant, BaA, BaP, BbF, BghiP, BkF, Chy, DbA, Fla, IdP, Phe, Pyr)	2011-2016	SPM	OSR monitoring program	Thollet et al., 2021; Delile et al., 2020.

	Σ_7 PCB		Σ_{12} PAH		Cd		Cr		Hg		Pb		Zn		Cu		Ni		Mean TME		SPM
	ΔC	ΔF	ΔC	ΔF	ΔC	ΔF	ΔC	ΔF	ΔC	ΔF	ΔC	ΔF	ΔC	ΔF	ΔC	ΔF	ΔC	ΔF	ΔC	ΔF	
1980s-1990s	-58	-69			-35	-52	-66	-75	-76	-83	-36	-53	-37	-53	-26	-45	-21	-41	-42	-57	-26
1990s-2000s	-43	-59	-31	-50	-54	-67	+63	+18	-35	-53	-21	-43	-6	-32	-7	-33	+2	-26	-8	-34	-28
2000s-2010s	-35	-15	-45	-20	-25	-3	-15	+12	-4	+38	-3	+26	-3	+25	-15	+9	+8	+42	-8	+21	+44
$R_{C_{micropol}}$ vs. $R_{F_{micropol}}$	1.00		0.94		0.99		0.97		1.00		0.99		0.99		0.96		0.93				
$R_{F_{micropol}}$ vs. F_{SPM}	0.92		0.24		0.93		0.87		0.92		0.96		0.96		0.95		0.98				

Correlations in bold for p value ≤ 0.05

Or Peer Review